Female meiosis II and pronuclear fusion require Bicaudal-D

Paula Vazquez-Pianzola[1*], Dirk Beuchle[1], Gabriella Saro[1], Greco Hernández[2], Giovanna Maldonado[2], Dominique Brunßen[1], Peter Meister[1] and Beat Suter[1*].

[1] Institute of Cell Biology, University of Bern, 3012 Berne, Switzerland.

[2] Laboratory of Translation and Cancer, Unit of Biomedical Research on Cancer, Instituto Nacional de Cancerología (INCan), Mexico City, Mexico.

[*] Authors for correspondence: (beat.suter@izb.unibe.ch, paula.vazquez@izb.unibe.ch)

keywords: *Drosophila* meiosis, mitosis, spindle assembly, clathrin, Bicaudal-D, BicD, TACC, CH-TOG, microtubule transport, deGradFP.

Running title: zygote formation requires *BicD.*

ABSTRACT

Drosophila Clathrin heavy chain (Chc) is transported by the dynein/dynactin microtubule motor through its interaction with the adaptor protein Bicaudal-D (BicD). Here we show that *Drosophila* BicD and Chc localize to centrosomes and spindles during mitosis and to the tandem spindles during female meiosis II. Reducing the activity of BicD::GFP specifically in freshly laid eggs revealed that BicD is essential for the production of normal female meiosis II products and for pronuclear fusion. Chc interacts with BicD and D-TACC, and BicD is needed to correctly localize the microtubule-stabilizing factors D-TACC, clathrin, and Msps to the meiosis II spindles, suggesting that BicD acts by localizing these proteins. In unfertilized eggs, reduced BicD levels cause the female meiotic products to re-enter the cell cycle. As BicD is required to localize the spindle assembly checkpoint (SAC) components Mad2 and BubR1 to the female meiotic products, it appears that BicD functions to localize them to control metaphase arrest of polar bodies. Finally, *Drosophila* and *C. elegans* orthologs of *BicD* and *tacc* are also needed for pronuclear fusion.

INTRODUCTION

Encoded by a single gene, the *Drosophila* BicD protein is part of a family of evolutionarily conserved dynein adaptors responsible for the transport of different cargoes along microtubules (Vazquez-Pianzola et al., 2016; Hoogenraad and Akhmanova, 2016; Vazquez-Pianzola and Suter, 2012). The founding member of this protein family, *Drosophila* BicD, was identified because of its essential role during oogenesis and embryo development where it transports mRNAs which control polarity and cell fate (Bullock and Ish-Horowicz, 2001; Suter and Steward, 1991; Suter et al., 1989; Wharton and Struhl, 1989). This process is mediated by its binding to the RNA-binding protein Egalitarian (Egl) (Dienstbier et al., 2009; Mach and Lehmann, 1997). In the meantime, BicD and its orthologs have been shown to control a diverse group of microtubule transport processes through binding to different

cargoes or adaptor proteins (Hoogenraad and Akhmanova, 2016; Vazquez-Pianzola and Suter, 2012).

BicD can alternatively bind to Chc and this interaction facilitates Chc transport of recycling vesicles at the neuromuscular junctions and regulates endocytosis and the assembly of the pole plasm during oogenesis (Li et al., 2010; Vazquez-Pianzola et al., 2014). The best-known function of Chc is in receptor-mediated endocytosis as part of clathrin, a trimeric scaffold protein (called triskelion), composed of three Chc and three Clathrin light chains (Clc) (Brodsky, 2012). Aside from this, clathrin was shown to localize to mitotic spindles in mammalian and *Xenopus* cells (Fu et al., 2010; Royle et al., 2005) and to possess a non-canonical activity by stabilizing the spindle microtubules during mitosis (Royle, 2012). This function depends on clathrin trimerization and its interaction with Aurora A-phosphorylated Transforming Acidic Coiled-Coil protein 3 (TACC3) and the protein product of the colonic hepatic Tumor Overexpressed Gene (ch-TOG) (Booth et al., 2011; Fu et al., 2010; Lin et al., 2010; Royle and Lagnado, 2006; Royle et al., 2005). This heterotrimer forms inter microtubule bridges between Kinetochore-fibers (K-fibers), stabilizing these fibers and promoting chromosome congression (Booth et al., 2011; Royle et al., 2005). More recently, TACC3 and a mammalian homolog of Chc (CHC17) were shown to control the formation of a new liquid-like spindle domain (LISD) that promotes the assembly of acentrosomal mammalian oocyte spindles (So et al., 2019).

As *Drosophila* BicD forms complexes with both Chc and Dynein, two proteins with essential mitotic and meiotic activities, we set out to investigate possible *BicD* functions during cell division. BicD and Chc localize to the mitotic spindles and centrosomes, but also to the female tandem meiotic II spindles. Reduced BicD levels revealed that BicD is needed to correctly localize D-TACC, clathrin, and Msps (ch-TOG homolog) to the meiosis II spindles and for normal progression of meiosis II. BicD is required for the normal metaphase arrest of polar bodies after meiosis II completion and our results suggest that this activity is mediated by BicD's role in localizing the spindle assembly checkpoint (SAC) components. Interestingly, *BicD* and *tacc* are also needed for pronuclear fusion after fertilization.

76 **RESULTS**

77 **BicD and its cargo clathrin localize to centrosomes and spindles during mitosis and to**
78 **tandem spindles in meiosis II**

79 Completion of female meiosis and the first mitotic cycles depend on the correct spindle
80 formation in the egg and the developing embryo. Maternally expressed genes provide all the
81 proteins that control these processes, and their inactivation leads either to maternal effect
82 lethality or female sterility. Indeed, *BicD* loss-of-function mutants are female sterile because
83 they do not produce oocytes (Ran et al., 1994). This is an obstacle for studying the role of
84 *BicD* in the maternally controlled early mitotic divisions of the embryo. Our laboratory has
85 developed the $BicD^{mom}$ females, a method to overcome *BicD* mutant female sterility (Swan
86 and Suter, 1996). In $BicD^{mom}$ females, BicD is provided from an inducible promoter that can
87 be turned off once oocyte fate is established. Around 3-4 days after shutting down *BicD*,
88 $BicD^{mom}$ ovaries contain egg chambers devoid of BicD and few of them develop into eggs
89 (Swan and Suter, 1996; Vazquez-Pianzola et al., 2014). Using this strategy, we observed that
90 the eggs laid by $BicD^{mom}$ females did not develop but arrested during stage 1 with phenotypes
91 that required a more detailed analysis (see below) (Fig. S1A and SM1-4). This suggests that
92 *BicD* is also essential downstream of oocyte differentiation to complete meiosis and progress
93 through the early mitotic divisions.

94 We analyzed BicD localization during mitosis in methanol-fixed embryos. Methanol
95 fixation dissolves the cytosolic pool of BicD, making insoluble pools of the protein more
96 apparent. Surprisingly, during the syncytial divisions, BicD was detected on the centrosomes
97 where it colocalized with the pericentrosomal marker centrosomin (Cnn), as well as on
98 mitotic spindles (Fig. 1A,a,b, Fig. S1B). During cellularization, BicD was additionally
99 enriched at the plasma membrane (Figure 1Ac). To confirm the specificity of the BicD
100 antibody, we additionally analyzed embryos expressing BicD::GFP by immunofluorescence
101 after staining them with anti-GFP. Both staining patterns were highly similar (Fig. 1B and
102 Fig. S1C).

Chc is also present at the mitotic apparatus in vertebrates (Fu et al., 2010; Royle et al., 2005) and *Drosophila* Chc is transported by BicD (Li et al., 2010; Vazquez-Pianzola et al., 2014). Because available antibodies against Chc do not work well for immunostaining (Li et al., 2010), we analyzed the expression of the Chc in *Drosophila* embryos using tagged, yet functional, Chc fusions (Vazquez-Pianzola et al., 2014). Both, immunostaining of different tagged Chc proteins (Fig. 1C, Fig. S2A, Fig. S2B) and live imaging of embryos expressing fluorescent Chc (Fig.1D, Fig. S2C) revealed that Chc, like BicD, was enriched at the centrosomes and pericentrosomal regions during the entire cell cycle where it also co-localized with Cnn (Fig. 1C and Fig. S2B). During mitosis, Chc associates in addition with the mitotic spindles (Fig. 1C,D and Fig. S2C). This pattern of localization was not an overexpression artifact, because the localization of a Flag-tagged Chc expressed under its own promoter in a *Chc* null background, showed the same localization pattern (Fig. S2B). Moreover, similar to BicD, Chc was also enriched during cellularization near the plasma membrane between the nuclei, probably marking the sites where endocytic vesicles start to form (Fig. 1C) (Sokac and Wieschaus, 2008). A similar overall localization pattern was observed for the *Drosophila* Clathrin light chain (Clc) during embryogenesis (Fig. S2D). Interestingly, Chc was not only present at the mitotic spindles but also localized to the first spindles observed in the laid eggs, the female meiotic II tandem spindles. Chc signal was detected on both tandem spindles and the central aster (Fig. 1E). Assessing the localization of BicD in freshly laid eggs was challenging because of the high levels of BicD in the cytoplasm. Using the anti-BicD antibody, we observed a specific BicD signal, but this was at the same level in the meiotic spindle region as in the cytoplasm (Fig S1D). However, the presence of BicD at the meiotic spindle was more clearly detected with the anti-GFP antibody in *BicD::GFP, BicD*^{null} eggs. Similar to Chc, BicD::GFP was enriched above cytoplasmic levels on the meiotic tandem spindles and the central aster (Fig. 1F, and Fig. S1E,E').

We conclude that BicD and Chc associate with the mitotic spindles and the centrosomal region during mitosis and with the tandem spindles and the central aster during female meiosis II. Thus, the localization of the Chc/Clc complex to the mitotic apparatus appears to

be conserved between *Drosophila* and mammalian cells (Royle et al., 2005). Interestingly, mammalian BicD1 and BicD2 are present at the centrosomes in mammalian cells as well (Fumoto et al., 2006). Therefore, our data suggest that *BicD* might play a yet unidentified, but evolutionarily conserved role at the mitotic/meiotic spindles.

deGradFP knockdown of BicD::GFP reveals a novel, essential role for BicD during early embryogenesis

Although $BicD^{mom}$ flies lay embryos with mitotic defects, the number of eggs they lay is too small for phenotypic analyses. Thus, we designed a strategy to knock down the BicD protein directly in young embryos (stage 1) using the deGradFP technique (degrade Green Fluorescent Protein), a method to target fusion proteins with GFP for destruction or inactivation (Caussinus et al., 2011). For this, we took advantage of the functional, genomic *BicD::GFP* construct (Paré and Suter, 2000). Additionally, we constructed a deGradFP system specifically active during embryogenesis but not oogenesis by expressing the deGradFP (NSlmb-vhhGFP4) from a *hunchback* (*hb*) minimal maternal promoter coupled with the *bcd* 3'-UTR (Fig. 2A). The *hb* promoter is active during late oogenesis such that the *deGradFP* mRNA will be loaded into eggs and embryos. The *bcd* 3' UTR promotes mRNA localization to the anterior pole of the oocyte and egg, and allows translation only upon egg activation in freshly laid eggs (Berleth et al., 1988; Driever and Nüsslein-Volhard, 1988; Sallés et al., 1994). We refer to this construct as *hb-deGradFP* (Fig. 2A). We corroborated the enrichment of the *deGradFP* mRNA in the anterior region of the embryo from egg-laying until before cellularization (Fig. 2B). Immunostaining experiments to detected *hb-deGradFP* expression revealed that the Vhh-GFP was distributed throughout the embryo and did not form an A-P gradient (Fig. 2C). It thus appears that the deGradFP is stable and can move to the rest of the embryo. Our new *hb-deGradFP* tool should therefore be useful to degrade GFP fusion proteins in entire young embryos.

157 A previously described *BicD::GFP* construct rescued the sterility phenotype and the
158 embryonic developmental arrest of *BicD* loss-of-function mutant females (*BicD::GFP,*
159 $BicD^{null}$ homozygous females) (Paré and Suter, 2000) (Fig. 2D-E). However, when these
160 females expressed 2 copies of the *hb-deGradFP* construct (*BicD::GFP,* $BicD^{null}$; *hb-*
161 *deGradFP* homozygous females), 75% of their progeny failed to developed into late
162 embryonic stages and did not hatch into larvae, showing, instead, arrest in meiosis or the first
163 mitotic divisions as observed in embryos laid by $BicD^{mom}$ females (Fig. 2D-E, Fig. SM5-7. In
164 the following, we will refer to these progeny and their mothers as $BicD^{hb\text{-}deGradFP}$. Embryos
165 laid by females that expressed two copies of the *hb-deGradFP,* but also a wild-type $BicD^{+}$
166 (*BicD::GFP,* $BicD^{null}$/+(CyO); *hb-deGradFP*), did not show developmental problems,
167 indicating that high levels of *hb-deGradFP* expression are not deleterious for development on
168 their own (Fig. 2D-E). As assayed by immunofluorescence and Western blotting, $BicD^{hb-}$
169 ^{deGradFP} females displayed normal ovaries and their BicD::GFP protein levels were not
170 noticeably reduced in the ovary (Fig. 2F-H), confirming that the *hb-deGradFP* construct is
171 not active during oogenesis. In contrast, in young $BicD^{hb\text{-}deGradFP}$ embryos, the BicD::GFP
172 signal was clearly reduced in the entire embryo (Fig. 2G) and BicD::GFP protein levels were
173 downregulated by 50% (Fig. 2I). BicD::GFP is expressed at levels comparable to the wild-
174 type BicD protein (Fig. S3A). However, 50% reduction in the levels of BicD::GFP protein
175 detected by WB produces already visible phenotypes, while eggs from heterozygous females
176 ($BicD^{null}$/+) that have also a 50% reduction of BicD compared to wild-type embryos (Fig
177 S3A) develop normally (97.3 ±1.03 % embryos hatched into larvae). Although alternative
178 explanations for these differences are possible, we think that the deGradFP might bind
179 BicD::GFP, functionally inactivating the protein before sending it to degradation.

180 As intended, the *hb-deGradFP* construct is expressed much higher in young embryos
181 than in ovaries, although low levels of expression were also seen in ovaries (Fig. 2H, I) and
182 even when these were dissected in the hypotonic Robbs medium that is normally used to
183 avoid oocyte activation (Fig. S4A). Although we cannot rule out that some old egg chambers
184 are activated during dissection due to physical activation, it is also possible that the *bcd* 3'-

185 UTR sequence is not sufficient to fully control translation in the context of the maternal *hb*
186 promoter and its 5'-UTR. Stage 14 (S14) oocytes are normally arrested in Metaphase I of
187 meiosis I until the oocyte becomes activated by its passage through the oviduct. Because
188 BicD is also present at the MI spindles in S14 oocytes (Fig. S4B), we further assessed the
189 specificity of the early embryonic effect of $BicD^{hb\text{-}deGradFP}$ by looking for evidence that $BicD^{hb\text{-}}$
190 ^{deGradFP} causes meiosis I defects in oocytes (Fig. S4C-D). However, $BicD^{hb\text{-}deGradFP}$ S14
191 oocytes displayed no evident problems in spindle formation or chromosome alignment in
192 meiotic metaphase I, suggesting that the early embryonic arrest observed in $BicD^{hb\text{-}deGradFP}$
193 individuals is not due to earlier meiotic defects during late oogenesis.
194

195 ***BicD* is required for the cell cycle arrest of the male and the female meiotic products,**
196 **and for pronuclear fusion**

197 To learn more about the novel BicD function in the earliest phase of embryonic development
198 (Fig. 3) and to pinpoint the developmental stage, we collected fully viable control embryos
199 and $BicD^{hb\text{-}deGradFP}$ embryos over a 30 min period, let them develop for another 30 min (30-60
200 min old collections) and analyzed them for developmental defects (Fig. 3A). Twenty-five
201 minutes after the eggs were laid, control embryos finished the 2nd mitotic division and
202 contained at least four zygotic nuclei. At this early stage, normal zygotic nuclei reside in the
203 interior of the embryo and the three remaining female meiotic polar body products (mostly
204 fused into one or two rosette-shaped nuclei) reside at the embryonic surface. Indeed, most
205 embryos laid by control mothers (*BicD::GFP,* $BicD^{null}$ or *BicD::GFP,* $BicD^{null}$ / + (CyO); *hb-*
206 *deGradFP)* developed normally, displaying more than four zygotic nuclei with normally
207 looking mitotic spindles (Fig. 3A-B). However, embryos laid by $BicD^{hb\text{-}deGradFP}$ mothers were
208 arrested mostly at earlier stages, displaying spindle-like structures that appeared abnormal
209 (Fig. 3A, C). Even though they contained mainly centrally located dividing nuclei, around
210 25% of these embryos were classified as "arrested with centrosomes" because they were
211 positive for Cnn staining (Fig. 3A, an example in Fig 3Ca). In this category, we found

212 embryos that contained at least one spindle displaying clear and sometimes fragmented
213 staining for the centrosomal marker centrosomin (Cnn) at the spindle poles. Additionally,
214 they frequently also displayed "free centrosomes" marked by Cnn signals associated with α-
215 tubulin, but without a complete spindle and without DNA (example in Fig. 3Ca1). Embryos
216 displaying acentrosomal spindles but containing free centrosomes were also scored into this
217 category. Another 35% of the *BicD*$^{hb\text{-}deGradFP}$ embryos possessed one or more internal
218 acentrosomal spindle and all these spindles were negative for Cnn staining and were classified
219 as "arrested, acentrosomal" (Fig. 3A, Cb).

220 Consistent with the fact that centrosomes are inherited from the father, embryos
221 arrested and classified as "arrested with centrosomes" were mostly marked by the presence of
222 the sperm tail (Fig. S5A-B). In contrast, embryos displaying "acentrosomal"-like spindles and
223 no free centrosomes rarely displayed any of these sperm tail markers, indicating that they
224 more likely represent unfertilized eggs with aberrant meiotic products (Fig. S5A-B). We then
225 analyzed in more detail the phenotype of arrested fertilized *BicD*$^{hb\text{-}deGradFP}$ eggs by detecting
226 the presence of the X and Y chromosomes by DNA fluorescent *in situ* hybridization (FISH).
227 Male embryos (marked by the presence of the Y) develop only from fertilized eggs. Male
228 embryos from control mothers showed one dot-like signal for the X chromosome and one
229 signal for the Y in each zygotic nucleus, and these nuclei were located in the interior of the
230 embryo (Fig. 3D1). The three polar bodies, formed after the two meiotic divisions, normally
231 fused into a single polar body that was marked by the presence of the 3 X chromosomes (Fig.
232 3D2). In contrast, all arrested male embryos laid by *BicD*$^{hb\text{-}deGradFP}$ females had at least one
233 internal spindle marked only by the presence of the Y chromosome and no X chromosome
234 signal, indicating that pronuclear fusion failed to take place and that a spindle still formed
235 from the paternal pronucleus (Fig. 3E-G). In most of these embryos, the male pronucleus
236 underwent only one additional round of replication since two dots of the Y chromosome
237 signal can be observed in the internal metaphase spindle (70 %, Fig. 3E3). Embryos with
238 more than one paternal spindle and many Y chromosome signals were also observed at a

239 lower frequency (30%, Fig 3F2-3,G4-6). Independent of the rounds of replication observed in
240 the parental pronucleus, these arrested *BicD*$^{hb\text{-}deGradFP}$ embryos also contained one or several
241 acentrosomal nuclei marked frequently by the presence of several dots of X chromosomal
242 signal, suggesting that the polar bodies did not arrest in metaphase II as they normally do but
243 underwent several cycles of DNA replication instead (example in Fig. 3E1-2, 3F1, 3G1-4).
244 These results show that *BicD* is required for the female and male pronucleus cell cycle arrest
245 and for pronuclear fusion.
246

247 **BicD is needed for replication arrest of the polar bodies and for their rosette formation**

248 To test for an essential function of *BicD* during the final phase of the meiotic divisions, we
249 crossed *BicD*$^{hb\text{-}deGradFP}$ and control females to sterile XO males, causing them to lay
250 unfertilized eggs (Fig. 4). In wild-type unfertilized eggs, egg activation is triggered by
251 passage through the oviduct, and this causes the eggs to complete meiosis II. In collections of
252 0-1h old unfertilized control eggs, we observed from 1 to 4 rosette-like nuclei. These
253 represent intermediate stages of the fusion process of the four meiotic products, which
254 ultimately fused to form a single, rosette-shaped nucleus in wild-type eggs indicating that
255 eggs completed meiosis II. These rosette-shaped nuclei were also marked by the presence of a
256 total number of 4 dots of X-chromosomal signal per egg, which arise from each of the four
257 meiotic products (Fig. 4A, examples in Fig. 4B). In contrast, *BicD*$^{hb\text{-}deGradFP}$ unfertilized eggs
258 contained one to several nuclei forming spindle-like structures, mostly with the appearance of
259 multipolar spindles (Fig. 4A). Additionally, their chromosomes did not create a rosette
260 structure that would be typical for a metaphase arrested state. Instead, these nuclei displayed
261 partially decondensed chromatin, an irregular shape, and they lacked the α-tubulin staining
262 ring that surrounds the DNA rosette in control eggs (Fig. 4A,C). Furthermore, the X-
263 chromosomal probe produced more than the normal four signal dots per egg, in eggs
264 containing only one nucleus (Fig. 4C-c) and in eggs containing several nuclei and spindles
265 (Fig. 4C-c'). We also observed eggs with more than four meiotic nuclei (like in Fig. 4Cc'),

266 indicating that *BicD*$^{hb\text{-}deGradFP}$ eggs show over-replication of the meiotic products. The probe
267 used for the FISH experiments recognizes a repetitive region on the X chromosome present
268 along 3 to 3.5 Mb. The fact that this probe detected more than four signals in each *BicD*$^{hb\text{-}}$
269 ^{deGradFP} egg, and that these signals showed different brightness and sizes might also suggest
270 that the DNA has become fragmented and/or more decondensed and that it did not arrest in a
271 metaphase-like state as in the normal rosette structures. This replication, decondensation
272 and/or fragmentation of the meiotic DNA was not restricted to the sex chromosomes because
273 we observed analogously additional signals when using a probe for the 2nd chromosome (Fig.
274 S6). Altogether, these results indicate that BicD is required for both the replication arrest and
275 the formation of the typical rosette-like structures of the polar bodies.
276

277 **Role of BicD in SAC and metaphase arrest of female meiotic products**

278 After meiosis II is completed, *Drosophila* polar bodies remain arrested in a metaphase-like
279 state. In wild-type unfertilized eggs, the four meiotic products, which fused into a single
280 rosette, showed strong signal for the mitotic marker Phospho-Histone 3 (PH3) along the entire
281 chromosomes, indicating that they were arrested in a metaphase-like state (Fig. 4Da-Ea). In
282 contrast, in *BicD*$^{hb\text{-}deGradFP}$ eggs showing one rosette-like structure, indicative of meiosis
283 completion, the PH3 staining was not localized along the entire chromosomes but only
284 enriched at the pericentromeric region (Fig. 4 Db-Eb). Moreover, their rosette-like structures
285 showed an increased number of CID-positive dots suggesting that female meiotic products
286 underwent extra rounds of replication/endoreplication (compare Fig. 4Da with 4Db).

287 Rosette-like structures in *BicD*$^{hb\text{-}deGradFP}$ eggs did also not form the typical tubulin ring
288 surrounding the chromosomes observed in wild-type eggs and, interestingly, DNA extended
289 beyond this tubulin ring and this DNA was negative for PH3 staining (Fig. 4Ea, b, c). In the
290 normal situation, Histone H3 phosphorylation starts in pericentromeric heterochromatin
291 regions at the onset of mitosis and then spreads along the entire length of chromosomal arms,
292 reaching its maximal abundance during metaphase. This is then followed by a rapid decrease

upon transition to anaphase (Sawicka and Seiser, 2012). Thus, PH3 staining confined to the pericentromeric region in *BicD*$^{hb\text{-}deGradFP}$ polar bodies suggests that these nuclei are not properly arrested or are released from metaphase arrest. Furthermore, *BicD*$^{hb\text{-}deGradFP}$ eggs possessing several meiotic products (Fig. 4Ec,c') showed that not all of these nuclei were positive for PH3 staining (Fig. 4Ec2-3,c'), further strengthening the idea that these nuclei are over-replicating due to a failure to arrest in metaphase.

The metaphase arrest of polar bodies depends on the activation of the spindle assembly checkpoint (SAC) pathway (Défachelles et al., 2015; Fischer et al., 2004; Pérez-Mongiovi et al., 2005). We, therefore, analyzed the localization of two well-conserved orthologs of the SAC pathway, BubR1, and Mad2 (Fig. 5). These proteins associate with unattached kinetochores and, in the case of BubR1, also to kinetochores lacking tension. By inhibiting the anaphase-promoting complex (APC/C) they are essential to maintain the metaphase arrest. BubR1 was clearly present at polar body kinetochores in the wild type (100%, n=23) and in the control BicD::GFP rescued eggs (93%, n=27) (Fig. 5Aa). However, in 43% of the *BicD*$^{hb\text{-}deGradFP}$ eggs, the meiotic products failed to recruit BubR1 to the kinetochores (n=35). The absence of BubR1 from the polar body kinetochores was observed in eggs where polar bodies were fused into a single rosette (Fig. 5Ab) and in eggs showing many additional meiotic products (Fig. 5Ad, d'). The rest of the *BicD*$^{hb\text{-}deGradFP}$ eggs showed either normal BubR1 recruitment (40%) or only a weak signal for kinetochore BubR1 (17%, Fig. 5Ac). These data indicate that the failure to activate or maintain the metaphase arrest of polar bodies in the absence of BicD is probably due to a failure to recruit the SAC components to the kinetochores or maintain their association. The fact that half of the polar bodies still recruited SAC components might also suggest that these nuclei are cycling in and out of the metaphase arrest, duplicating their chromosomes. Similar results were obtained for Mad2, where 69% of the *BicD*$^{hb\text{-}deGradFP}$ eggs analyzed did not show recruitment of Mad2 to the polar bodies (n=48; Fig. 5B). Altogether, these results suggest that in *BicD*$^{hb\text{-}deGradFP}$ eggs, the meiotic II products do not correctly arrest in metaphase due to a failure to activate or maintain the SAC.

321 **Proper localization of D-TACC, Msps, and Clc at tandem meiotic spindles requires BicD**

322 To pinpoint the first meiotic defects, we focused on the very early stages of meiosis II in eggs
323 that were just released from the MI arrest. The analysis of Chc distribution proved difficult
324 due to the lack of useful antibodies for immunostaining. Localization of tagged Chc was also
325 irreproducible due to the high cytoplasmic signal and the fact that overexpressing tagged Chc
326 in a background of reduced BicD levels increased the *BicD*$^{hb\text{-}deGradFP}$ phenotype (see Fig. 7C-
327 D). However, because the Chc partner Clc is also present at the mitotic spindles together with
328 Chc (Fig.S2D), we followed Clc localization during meiosis II. Clc localized to the female
329 MII tandem spindles and the central aster (Fig. 6A). Additionally, we detected an unusual,
330 strong accumulation of Clc at the central aster relative to the levels observed along the MII
331 spindles in *BicD*$^{hb\text{-}deGradFP}$ compared to control spindles (Fig. 6A, A'). We then followed the
332 localization of D-TACC and Msps (Mini spindles) because the spindle localization of their
333 mammalian homologs is interdependent with Chc (Royle, 2012; Royle et al., 2005). In wild-
334 type MII and anaphase II (AII) spindles, D-TACC and Msps were present on tandem
335 spindles, and they were enriched at the central aster (Fig. 6B, C arrowheads). In both
336 metaphase II and anaphase II, D-TACC is additionally weakly enriched at the spindles´
337 equator, where the MT plus ends are located (Fig. 6B, arrows). On the other hand, Msps was
338 clearly enriched along both arms of the tandem spindles but stained more strongly the minus
339 ends at the spindle poles (Fig. 6C, arrows). In *BicD*$^{hb\text{-}deGradFP}$ embryos, D-TACC and Msps
340 localization along the tandem spindles was generally clearly reduced compared to the control
341 spindles (Fig. 6B, C). However, like in control spindles, D-TACC and Msps still showed
342 enrichment at the central aster in *BicD*$^{hb\text{-}deGradFP}$ embryos (Fig. 6B, C). Accordingly, the signal
343 intensity for D-TACC and Msps along the most superficial tandem spindle relative to the
344 signal intensity observed in the central aster was significantly reduced in *BicD*$^{hb\text{-}deGradFP}$ MII
345 spindles (Fig 6B', C'). Thus, these results suggest that BicD is needed to properly localize
346 clathrin, D-TACC and Msps along the meiotic II spindles.
347

348 **Evidence for mutually exclusive complexes of BicD/Chc and D-TACC/Chc**

349 In mammals, Chc interacts directly with TACC3, and the interaction depends on the
350 phosphorylation of Ser^{552} of TACC3 by Aurora A (Fu et al., 2010; Lin et al., 2010). Since D-
351 TACC and clathrin fail to properly localize on $BicD^{hb\text{-}deGradFP}$ MII spindles, we further
352 investigated whether the *Drosophila* homologs of these proteins can interact with each other
353 and with BicD using a yeast 2-hybrid (Y2H) assay and co-immunoprecipitation experiments
354 (Fig. 7A-B). Indeed, full-length *Drosophila* Chc interacts with D-TACC in both assays.

355 The minimal region of mammalian isoform Chc22 that interacts with TACC3 consists
356 of amino acids 331-542 (Lin et al., 2010). Whereas the corresponding region of *Drosophila*
357 $Chc^{329\text{-}542}$ did not interacted with D-TACC in our assays (Fig. 7A), this region with a C-term
358 extension ($Chc^{329\text{-}803}$) interacted with D-TACC almost as strongly as the full-length protein
359 (Fig. 7A). Interestingly, $Chc^{329\text{-}542}$ was also unable to bind BicD (Fig. S7A), but $Chc^{329\text{-}803}$ had
360 been shown previously to contain the minimal BicD binding region (Li et al., 2010) (Fig.
361 S7B). $Chc^{329\text{-}803}$ interacted in our assays with the BicD CTD (C-terminal domain), a truncated
362 version of BicD that normally interacts stronger with its cargoes because it does not contain
363 the BicD fold-back domain (Fig. S7B) (Li et al., 2010). Since the sequences required for the
364 binding of *Drosophila* Chc to D-TACC and to BicD are overlapping, Chc/BicD and Chc/D-
365 TACC might only exist as mutually exclusive protein complexes. However, because Chc
366 normally acts as a trimer, higher-order complexes of the three Chc molecules could
367 theoretically contain BicD or D-TACC, or both. Surprisingly, the interaction of Chc with D-
368 TACC was not abolished when the conserved Ser residue targeted by the Aurora A kinase
369 was mutated to Alanine (Ser^{863} in D-TACC, corresponds to Ser^{552} of the human protein, Fig.
370 7A, Fig. S7C). Nevertheless, the phosphomimetic substitution Ser^{863}>Asp in D-TACC
371 increased its interaction with full-length Chc (Fig. S7C). These results suggest that
372 phosphorylation of Ser^{863} may not be a prerequisite for the interaction of full-length D-TACC
373 with Chc at least in the Y2H system. Still, it could enhance the interaction during mitosis and
374 meiosis when the kinase is active.

375 The interaction of D-TACC with full-length Chc was observed under very stringent
376 Y2H conditions (medium -L, -W, -H, -a; Fig. S7C). In contrast, the interaction between Chc
377 and BicD was only visible under less stringent conditions (medium -L, -W, -H +3 mM 3AT;
378 Fig. S7A, (Cagney et al., 2000)), suggesting that Chc interacts stronger with D-TACC than
379 with BicD in this system. This is also supported by the immunoprecipitation experiments
380 using embryo extracts. Using extracts expressing a Myc::Chc fusion protein, Myc::Chc was
381 observed at low levels in BicD IPs. In contrast, the presence of BicD was not detected in the
382 reverse IPs (with anti-Myc antibodies) as previously reported (Fig. 7B) (Vazquez-Pianzola et
383 al., 2014). This is conceivable due to their weak interaction or because the Myc tag interferes
384 with the binding sites. In contrast, D-TACC strongly co-immunoprecipitated with Myc::Chc.
385 On the other hand, no interaction was observed between D-TACC and BicD either by IP or
386 using the Y2H system (Fig. 7B, S7D).
387

388 **High levels of *Chc* enhance the embryonic arrest phenotype of *BicD*$^{hb\text{-}deGradFP}$ embryos**

389 *BicD::GFP, BicD*^{null} females, expressing only one copy of the *hb-deGradFP* construct
390 *(BicD::GFP, BicD*^{null}*; hb-deGradFP-bcd 3'UTR/+)* laid embryos that show a reduction of
391 BicD::GFP levels only by 30% on WB experiments, (Fig. S3B-C) and mostly developed
392 normally and hatched into larvae (Fig. 2D-E, 7C-D). However, when these females also
393 expressed a copy of a *Chc* transgene under the control of the strong maternal tubulin
394 promoter, 80% of their progeny failed to hatch as larvae and, instead, arrested with the same
395 abnormal nuclei phenotype observed in *BicD*$^{hb\text{-}deGRadFP}$ embryos (Fig. 7C-D). Overexpression
396 of this Chc construct alone did not produce visible phenotypes in embryos, suggesting that
397 high levels of Chc in a BicD-reduced background are responsible for the phenotype.
398
399
400
401

402 **Like BicD, *d-tacc* is required for pronuclear fusion and cell cycle arrest of the male**
403 **pronucleus and the female meiotic products**

404 *d-tacc*^{1} mutant mothers lay eggs with reduced D-TACC protein levels and most of these
405 embryos fail to develop (Gergely et al., 2000). Of the male progeny laid by *d-tacc*^{1}/
406 *Df(3R)110* females, only 25.8% showed signals for the X and Y chromosomes in each of their
407 zygotic nuclei, indicating that they had performed pronuclear fusion (Fig. S8A). The majority
408 of them (74.2%) had at least one internal nucleus strongly marked for the Y chromosome and
409 no X-chromosomal signal (Fig. S8 B-D,), even though, X chromosome signals strongly
410 marked the remaining nuclei which represent the female meiotic products. These data show
411 that in *d-tacc*^{1} embryos (Fig. S8), pronuclear fusion is strongly compromised. From these
412 embryos that did not perform pronuclear fusion, 30.4 % showed normal cell cycle arrest of
413 the female and male meiotic products (Fig. S8B). However, in the majority of them, the
414 paternal pronucleus underwent additional divisions with no over-replication of female meiotic
415 products (47.85 %, Fig. S8C). Only 21.7% *d-tacc*^{1} showed replication of the female meiotic
416 and male derived nuclei (Fig. S8D). The lower penetrance of this female meiosis phenotype
417 compared to the one observed in *BicD*$^{hb\text{-}deGRadFP}$ eggs (70% of the arrested eggs), could be
418 because *d-tacc*^{1} embryos produce high enough levels of D-TACC, sufficient to rescue the
419 female meiosis phenotype (Gergely et al., 2000). BicD and D-TACC are therefore needed for
420 pronuclear fusion and metaphase arrest of the male pronucleus and the female meiotic
421 products. Interestingly, we also observed abnormal meiosis with delayed polar body extrusion
422 in eggs from *C. elegans* worms fed with bacteria expressing dsRNA against *tac-1* (Fig. S9C).
423 Moreover, pointing to a conserved role for these proteins in pronuclear fusion, we found that
424 eggs from worms fed with dsRNA against *bicd-1, chc-1* and *tac-1* did not undergo pronuclear
425 fusion either (Fig. S9A-E).
426
427
428

429 **DISCUSSION**

430 **A useful strategy to study the effect of lethal or female sterile mutations in early**
431 **embryogenesis reveals that *BicD* is required for meiosis II and pronuclear fusion**

432 In this study, we found that BicD localizes to the female meiotic spindle during meiosis II,
433 where it is present at the tandem spindles and the central aster. After fertilization, BicD also
434 localizes to the mitotic spindles and the centrosomes. Since $BicD^{null}$ mutants rarely survive
435 and are sterile, we set up a strategy based on the deGDradFP technique to assess its role
436 during the early embryonic divisions. Using this strategy, we were able to generate embryos
437 with reduced levels of BicD at the very beginning of embryogenesis ($BicD^{hb\text{-}deGradFP}$ embryos).
438 Consistent with BicD localization at the female meiotic II spindles, we discovered that
439 $BicD^{hb\text{-}deGradFP}$ embryos arrest development displaying aberrant meiotic products and no
440 pronuclear fusion. Combined with the CRIPSP-Cas9 strategy first to produce functional GFP
441 tagged versions of the proteins of interest, the construct designed in this paper could be useful
442 to study the role of other female-sterile and lethal mutations during very early embryonic
443 development (Nag et al., 2018).
444

445 **Connecting BicD to the SAC pathway**

446 In unfertilized $BicD^{hb\text{-}deGradFP}$ eggs, the female meiotic products were not arrested in
447 metaphase as it normally happens. Instead, they underwent additional rounds of replication.
448 $BicD^{hb\text{-}deGradFP}$ female meiotic products failed to recruit or maintain the recruitment of the
449 SAC pathway components BubR1 and Mad2, which are normally present at the kinetochores
450 of the female meiotic polar bodies in wild-type eggs. Interestingly, in *Drosophila* mutants for
451 *Rod, mps1*, and *BubR1*, well-conserved orthologs of the SAC pathway, the polar bodies
452 cannot remain in a SAC-dependent metaphase-like state and decondense their chromatin, too
453 (Défachelles et al., 2015; Fischer et al., 2004; Pérez-Mongiovi et al., 2005). Furthermore, in
454 these mutants, the polar bodies have been shown to cycle in and out of M-phase, replicating

455 their chromosomes similarly to what we observed in *BicD*$^{hb\text{-}deGradFP}$ eggs. Thus, it appears that
456 BicD normally functions to localize these SAC components to induce and/or maintain the
457 metaphase arrest of the polar bodies. Several mechanisms could explain the failure to
458 maintain SAC activation observed in *BicD*$^{hb\text{-}deGradFP}$ embryos. BicD might be needed to recruit
459 the SAC components to kinetochores directly. On the other hand, during mitosis, dynein
460 motors have been shown to transport SAC components along the microtubules away from
461 kinetochores as a mechanism to trigger checkpoint silencing and anaphase onset (Basto et al.,
462 2004; Howell et al., 2001; Wojcik et al., 2001). Since BicD binds dynein, we expect that if
463 BicD acts as a linker to transport SAC components, it might be required to move them away
464 from the kinetochores. If this does not happen, the SAC remains persistently activated.
465 Whereas persistent SAC activation leads to metaphase arrest and delayed meiosis (D-
466 Meiosis), at least during mitosis, this delay is known to be rarely permanent. Most cells that
467 cannot satisfy the SAC, ultimately escape D-mitosis and enter G1 as tetraploid cells by a
468 mechanism that is poorly understood (Rieder and Maiato, 2004). Thus, it is possible that in
469 embryos with reduced *BicD* function, the SAC pathway is constantly activated, delaying
470 meiosis. However, at one point, the nuclei might escape the metaphase II arrest, cycling in
471 and out of M-phase, thereby replicating their chromosomes and de-condensing their
472 chromatin. The fact that female meiotic products in *BicD*$^{hb\text{-}deGradFP}$ embryos show no or only
473 pericentromeric PH3 staining and that they are replicating, supports the notion that these
474 nuclei are on an in-out metaphase arrest phase. This is also supported by the finding that the
475 meiotic products in around half of the *BicD*$^{hb\text{-}deGradFP}$ embryos failed to stain for the SAC
476 components BubR1 and Mad2.
477

478 **Connecting BicD to the D-TACC, Msps, and clathrin complex**

479 Chc is transported by BicD in oocytes and neurons and it shows a similar pattern of
480 localization as BicD (Li et al., 2010; Vazquez-Pianzola et al., 2014). During cellularization,
481 both are localized in a dotted pattern near the invaginating plasma membrane, probably

482 marking the sites where endocytic vesicles are formed. This is consistent with the described
483 role of BicD in regulating endocytosis in oocytes and neurons. During mitosis, Chc, its
484 partner Clc, and BicD are enriched at mitotic spindles and centrosomes. Furthermore,
485 clathrin, BicD, and the clathrin-interacting partners D-TACC and Msps localize to the tandem
486 spindles and the central aster of the female meiotic II apparatus. The interaction of
487 *Drosophila* Chc with D-TACC is conserved and Chc interacts through the same protein
488 domain directly with D-TACC and BicD (Fig 7, (Fu et al., 2010; Lin et al., 2010)).
489 Additionally, embryos laid by mothers overexpressing Chc in a background where BicD is
490 reduced down to levels that do not produce visible phenotypes on their own, also arrest during
491 early development. Moreover, BicD is needed for localizing normal levels of D-TACC, Msps,
492 and clathrin throughout the tandem spindles relative to their localization at the central aster
493 (Fig. 6). Thus, it appears possible that limited BicD activity in $BicD^{hb\text{-}deGradFP}$ embryos is
494 insufficient to localize clathrin, TACC, and Msps efficiently along the MTs of the spindle.
495 During mitosis, impairment of MT motors, such as dynein, as well as interference with MT
496 dynamics, persistently activates the SAC (Rieder and Maiato, 2004). Treatments that prevent
497 the TACC/ clathrin complex from binding to the mitotic spindles affect K-fiber stability and
498 persistently activate the SAC, too (Rieder and Maiato, 2004; Royle et al., 2005). As discussed
499 before, this SAC hyperactivation would also explain the over-replication of female meiotic
500 products observed in eggs with reduced BicD or D-TACC levels.
501

502 **Role of BicD in pronuclear fusion**

503 BicD is also needed for zygotes to perform pronuclear fusion (Fig 3). Furthermore, its role in
504 pronuclear fusion is conserved during evolution since *C. elegans* eggs depleted for *bicd-1* also
505 failed to undergo pronuclear fusion (Fig S9). Moreover, *Drosophila D-TACC* and *C. elegans*
506 *chc-1* and *tac-1* are also needed for pronuclear fusion (Fig S9). These genes might be required
507 indirectly, through their role in meiosis, since preliminary data also suggest that meiosis II is
508 compromised in *bicd-1* and *chc-1 ds*RNA fed worms (Fig S9). Alternatively, they might play

a more direct role in pronuclear migration, which is known to depend on Dynein and MTs in bovine, primate, and *C. elegans* embryos (Gönczy et al., 1999; Payne et al., 2003). Figuring out their precise mechanistic involvement in pronuclear fusion is an interesting question for further studies.

514 **MATERIALS AND METHODS**

515 ***Drosophila* stocks**

516 *P{matα4-GAL-VP16}*, *Nos-Gal4:Vp16* ; *UAS-Clc::GFP*, *Histone::RFP* ; C(1;Y)^1, y^{1}w: y$^+$/0
517 and *C(1)RM, y^1 v^1/0* stocks were obtained from the Bloomington *Drosophila* Stock Center
518 (NIH P400D018537), Flies containing the genome rescue transgenes p*CHC3+* (Bazinet et
519 al., 1993) and *4C-CHC* (Kasprowicz et al., 2008), were kindly provided by C. Bazinet and P.
520 Verstreken, respectively. *d-tacc^1* and *Df 3R(110),* covering the *tacc* locus, were provided by J.
521 Raff (Gergely et al., 2000). *UAS-Chc::eGFP* and *UAS-Chc::mcherry* flies (Li et al., 2010)
522 were provided by S. Bullock. Transgenic flies *pUASP-Chc-V5-K10-AttB*, and *pUASP-myc-*
523 *chc-K10-AttB* were described previously (Vazquez-Pianzola et al., 2014). *Df(2L)Exel7068*
524 (Exelixis) was used as *BicD* deficiency (BicD^{Df}). The *BicD^{null}* allele, *BicD^{r5}*, *Bic-D^{mom}*, and
525 *BicD::GFP* were described (Paré and Suter, 2000; Ran et al., 1994; Swan and Suter, 1996;
526 Vazquez-Pianzola et al., 2014). *White (w)* flies were used as controls.

527 For the production of unfertilized eggs, virgin *w* females were crossed to *C(1;Y)^1,*
528 *y^{1}w: y$^+$/0* males to generate XO males that are phenotypically normal but sterile. XO males
529 were then crossed to virgin females of the desired phenotype. Eggs laid by these females were
530 not fertilized.

531

532 **DNA constructs and generation of transgenic flies**

533 The generation of the flies expressing the *hb-deGRadFP* construct was as follows. We cloned
534 the NSlmb-vhhGFP4 sequence (that comprises the F-box domain contained in the N-terminal
535 region of the *Drosophila* supernumerary limbs (Slmb) protein fused to the GFP-binding
536 nanobody VhhGFP4 sequence) described by Caussinus and colleagues (Caussinus et al.,
537 2011) under the *hunchback* (*hb*) minimal maternal promoter containing the 5'-UTR leader of
538 the maternal 3.2 Kb *hb* transcript and combined it with the *bcd* 3'-UTR, following the
539 strategy used by Schulz and Tautz who used this to induce an artificial Hb gradient in

540 embryos (Schulz and Tautz, 1995). The *Nslmb-vhhGFP4* sequence was PCR-amplified with
541 specific primers bearing *BamHI* and *KpnI* sites using the plasmid pUAS-Nslmb-vhhGFP4 as
542 the template (Caussinus et al., 2011).

543 Primer sequences were the following ones. Nano-GFP-sense-BamHI
544 (GGATCCATGATGAAAATGGAGACTGACAAAAT) and Nano-GFP-anti-Kpn
545 (GGTACCTTAGCTGGAGACGGTGACCTGGGTG). PCR products were subcloned into
546 the same sites of the pCaSper-AttB vector to create the plasmid pCasper-AttB-Nslmb-
547 vhhGFP4 (or pw+GFP nanobody). A 1.5 Kbp fragment of the *bicoid* 3'-UTR genomic region
548 (Berleth et al., 1988) was amplified from a genomic library using specific primers containing
549 KpnI and NotI restrictions sites. Primers were: bcd 3'UTR sense-Kpn I
550 (GGTACCACGCGTAGAAAGTTAGGTCTAGTCC) and bcd 3'UTR anti-Not I
551 (GCGGCCGCGCTAGTGCTGCCTGTACAGTGTCT). The insert was cloned by T-end
552 ligation into the pCR2.1 TOPO vector and later subcloned into the KpnI/ NotI sites of
553 pCasper-AttB-Nslmb-vhhGFP4 to generate the pCasper-AttB-Nslmb-vhhGFP4-bcd 3'-UTR
554 construct (or pw+ GFP nanobody-bcd 3'-UTR). The minimal maternal *hunchback (hb)*
555 promoter region together with the 5'-UTR leader of the maternal 3.2 Kb *hb* transcript were
556 amplified using as template the Lac8.0 construct already described (Margolis et al., 1994) and
557 kindly provided by Jim Posakony. Primers for this amplification contained flanking BglII and
558 BamHI sites and were the following ones. Hb-pr-sense–BglII
559 (AGATCTTCCGGATCAGCGGCGCTGATCCTGC), and Hb-pr-Anti-BamHI
560 (GGATCCCTTGGCGGCTCTAGACGGCTTGCGGACAGTCCAAGTGCAATTC). Inserts
561 were further cloned into the *BamHI* of Nslmb-vhhGFP4-bcd 3'-UTR to generate Hb-Nslmb-
562 vhhGFP4-bcd 3'UTR (or pw+ Hb-GFP nanobody-bcd3'UTR). This final plasmid was
563 injected into embryos containing the ZH-attP-14/3R-86F landing platform to generate flies
564 expressing the *hb-deGradFP* construct.

565 The *Don Juan (Dj)::mCherry* construct to produce transgenic flies was generated as
566 follows. mCherry region was PCR-amplified with primers containing BamHI and HindIII

567 sites using pC4-SqhP-mCherry plasmid as the template (a gift from Romain Levayer). The
568 reverse primer added a GS-rich region to use as a linker and the stop codon was removed. The
569 amplified fragment was further subcloned into the BamHI/HindIII sites of the plasmid
570 *pw+SNattB* (Koch et al., 2009) to generate the plasmid *pw+attB*-mCherry. The genomic
571 region containing the minimal promoter, the 5'-UTR, and the ORF of *Dj* gene was PCR-
572 amplified from genomic fly DNA using primers containing EcoRI and BamHI sites, and
573 cloned into the same sites of *pw+attB*-mCherry to generate the final construct *pw+attB - Don*
574 *Juan (Dj)::mCherry.* This construct was further injected into flies containing the ZH-attP-52 /
575 3L-64A landing platform for transgenesis.
576

577 **Hatching rate determination and embryo development**

578 Hatching rates were scored as follows. Virgin females of the desired genotype were crossed to
579 control *white* males. Females were allowed to lay eggs on agar plates for several hours or
580 overnight. Around 100-200 embryos were marked in the plate and further developed for 48 h
581 at 25°C. After 48 h, embryos that did not hatch were counted. For scoring embryo
582 development, 30 min to 60 min or 2- to 5h old embryos were collected. Embryos were then
583 fixed and stained to detect both α-tubulin and DNA to score the development stage.
584

585 **Western blots**

586 The preparation of ovaries for Western blots was as follows. Seven pairs of ovaries were
587 collected in 20 µl of SDS-sample buffer, boiled for 2 min., vortexed for 15 sec., boiled for
588 another 8 min. Finally, they were loaded onto an SDS –PAGE. Western blots were performed
589 using mouse monoclonal anti-BicD antibodies (a mixture of 1B11 and 4C2, 1:10 dilution,
590 (Suter and Steward, 1991), mouse anti-α-tubulin (1:2,000 dilution of the cell culture´s
591 supernatant, Developmental Studies Hybridoma Bank (DSHB)), rabbit anti-mammalian Chc
592 (1:500 dilution, (Hirst et al., 2009)), rabbit anti-GFP (1:3,000 dilution, Immunokontact),
593 rabbit anti-Clc (1:3,000, (Heerssen et al., 2008)), mouse monoclonal anti-Myc 9E10 (1:5 cell

594 culture supernatant, DSHB), and rabbit anti D-TACC (1:10,000 dilution, (Kao and Megraw,
595 2009)). Primary antibodies were detected using horseradish peroxidase-conjugated secondary
596 antibodies (GE Healthcare). To detect the deGRadFP expression from the *hb-deGRadFP*
597 construct, anti-llama IgG-heavy and light chain antibodies (1:500 dilution, Bethyl) were used
598 and developed using anti-goat IgG (H+L)-HRP conjugated antibodies (1:500 dilution,
599 Invitrogen).
600
601 **Immunoprecipitations (IPs)**

602 IPs were done essentially as previously described (Vazquez-Pianzola et al., 2011). 30 µl of
603 protein-G Sepharose beads (Amersham) and 1 ml of embryo extracts were used per IP.
604 Extracts were prepared from 0-20 h old embryos expressing a Chc::Myc fusion protein under
605 a maternal Tubulin promoter. As a negative control, extracts were also prepared from wild-
606 type embryos (OreR). For each IP, 1 ml of cell culture supernatant of monoclonal anti-BicD
607 1B11, anti-BicD 4C2, or anti-Myc 9E10 antibodies were bound to the beads. To IP TACC, a
608 solution containing 2 µl of the polyclonal anti-TACC UT316 antibody (Kao and Megraw,
609 2009) diluted in 1 ml of PBS was used to bind to the protein-G beads. Beads were
610 resuspended in 30 µl of sample buffer, and 7 to 15 µl per well was analyzed by Western blot.
611
612 **Immunostainings**

613 Immunostainings of embryos were done using the following primary antibodies: mouse anti-
614 BicD (a mix of 1B11 and 4C2, 1:10 dilution), mouse anti-Myc 9E10 (dilution 1:5, DSHB),
615 mouse anti-Flag (1:200, Sigma), mouse anti-V5 (1:200, Invitrogen), rabbit anti-Cnn (1:500
616 (Heuer et al., 1995)), rabbit anti Clc (1:500 (Heerssen et al., 2008)), mouse monoclonal anti-
617 α-tubulin DM1A (1:500, Sigma), rabbit anti α-tubulin (1:500, Abcam), rabbit anti-GFP
618 (1:300, previously preabsorbed on embryos, Immunokontakt), rabbit anti D-TACC UT316
619 (1:1,000 (Kao and Megraw, 2009)), rabbit anti D-TACC (1:500 (Gergely et al., 2000)), rabbit
620 anti-Msps (1:500 (Cullen et al., 1999)), mouse anti-Flag (1:200, Sigma, F3165) , rabbit anti

621 CID (1:400 (Buster et al., 2013)), rabbit anti p-Histone H3 (S10) (1:200, Cell Signalling),
622 mouse anti p-Histone H3 (1:200, Cell Signalling), rabbit anti BubR1 (1:2,000 (Logarinho et
623 al., 2004)), and rabbit anti Mad2 (1/1,000 (Logarinho et al., 2004)). To detect the hb-
624 deGRadFP construct, anti-llama IgG-heavy and light chain (1:500 dilution, Bethyl) was
625 developed anti-goat Alexa Fluor 680 (H+L) (Ivitrogen).

626 Secondary antibodies used were Cy3-conjugated goat anti-mouse, DyLight 647-
627 conjugated goat anti-mouse or anti-rabbit antibodies (Jackson Immunoresearch), A488-
628 conjugated goat anti-rabbit (Molecular Probes), Oregon Green 488 conjugated goat anti-
629 mouse (Molecular Probes), donkey anti-mouse AF488 (Molecular Probes), AF568 conjugated
630 donkey anti-mouse, and AF488 conjugated donkey anti-rabbit A488 (Molecular Probes).
631 Nuclei were visualized by staining DNA with 2.5 µg/ml Hoechst 33258 (Molecular Probes)
632 for 40 minutes during the final wash or incubated overnight when early meiosis in embryos
633 was analyzed. Control immunostainings using only secondary antibodies were performed to
634 detect unspecific binding of the secondary antibodies. For co-localization studies, control
635 samples using only one of the primary antibodies and both secondary antibodies were
636 performed to detect bleed through to the other channel. When detecting tagged proteins,
637 samples of wild-type specimens were used as a control for unspecific binding of the anti-tag
638 antibody. Embryos were either fixed with 4% paraformaldehyde (PFA) or with methanol, as
639 indicated. Methanol fixation was mainly used to preserve the cytoskeleton structure and or
640 reduce the cytoplasmic levels in BicD staining. Methanol fixation was done as previously
641 described (Kellogg et al., 1988). When antigens were not well preserved in methanol fixations
642 (for example, this was observed for the Chc fusion proteins), fixation with 4%
643 paraformaldehyde (PFA) was used. To detect endogenous BicD::GFP in ovaries, ovaries were
644 fixed with 4% PFA. For preserving the endogenous Clc::GFP signal, embryos were hand-
645 devitellinized and fixed in a mixture of Heptane saturated with PFA for 15 min. For
646 preserving the Dj:mcherry and Chc::mCherry signal, the embryos were fixed with MetOH.
647 Stage 14 oocytes for immunostainings were prepared as previously described (Radford and
648 McKim, 2016).

649 Images were analyzed with a Leica TCS-SP8 confocal microscope. Most of the
650 spindle pictures represent Z-stack maximal intensity projections along the frames. MII and
651 Anaphase II images were acquired such that the central aster signal was highest, but bellow
652 saturation. Due to the strong/robust Clc signal in the cytoplasm, the spindle perpendicular
653 position to the surface and the depth of the sample, it was not possible to analyze Clc
654 localization at the different regions of the meiotic spindles by directly analyzing the Z-stack
655 of maximal confocal projection images. The high cytoplasmic signal in the first planes
656 masked the localization at the spindle in the deeper planes. Thus, to detect the presence of
657 Clc along the tandem meiosis spindles, Z-stack images were processed to correct for depth
658 and bleaching in Image J. All stacks were processed the same way. First, a crop area
659 corresponding to the spindle of the same size was cropped in each image. Channels were then
660 split and subjected to corrections separately. Each channel was smooth with a median filter
661 radius of 1 to decrease the noise. The channel corresponding to the Clc staining had the most
662 robust signal intensity loss through the sample´s depth. This channel was subject to bleach
663 correction with a simple ratio fit to compensate for intensity attenuation in the image´s deeper
664 stacks. Channels corresponding to α-tubulin and DNA staining did not lose so much intensity
665 with the sample´s depth. They were subjected to an attenuation correction using an ImageJ
666 plugin already described (Biot et al., 2008). After intensity correction, the final image was
667 created by merging the channels previously subjected to maximal intensity Z-stack projection.
668

669 **Fluorescent *in situ* hybridization (FISH)**

670 For mRNA FISH, RNA probes were prepared and hybridization experiments were performed
671 as previously described (Vazquez-Pianzola et al., 2017). To detect deGRadFP mRNA, the
672 *VhhGFP4* region of the *hb-deGRadFP* transgene was first amplified by PCR with primers
673 containing T3 and T7 promoter sequences, and the plasmid pUAS-Nslmb-vhhGFP4 as a
674 template (Caussinus et al., 2011). Primer sequences were the following ones. The sense
675 primer containing the T3 promoter was:

676 GGGGGGAATTAACCCTCACTAAAGGGAGAATGGATCAAGTCCAACTGGTGGAGT
677 and the antisense primer containing the T7 promoter was:
678 GGGGGGTAATACGACTCACTATAGGGAGATTAGCTGGAGACGGTGACCTGGGTG.
679 Antisense and sense probes were generated using T7 and T3 RNA polymerase, respectively.
680 A sense probe was used to detect unspecific background.
681 DNA FISH to *Drosophila* chromosomes was done mainly according to (Dernburg, 2000).
682 DNA oligos hybridizing to repetitive regions of the Y $(AATAC)_6$ and the 2nd chromosome
683 $(AACAC)_7$ were ordered modified with Cy3 and Cy5 fluorophores at their 5' end,
684 respectively, from Microsynth. The sequences were already described (Dernburg, 2000). The
685 sequence used to detect the X chromosome by hybridizing to TTT-TCC-AAA-TTT-CGG-
686 TCA-TCA-AAT-AAT-CAT recognizes the 359-bp satellite block on the *D. melanogaster* X
687 chromosome as well as minor variants on chromosome 3 was described by (Ferree and
688 Barbash, 2009). A 5' end Cy5 fluorophore-labeled probe was used. Embryos were fixed with
689 methanol for DNA FISH. Probes were used at a final concentration of 5 ng/µl in hybridization
690 buffer. The blocking buffer used (before adding the first antibody for detection of the desired
691 proteins) was: 2x SSC, 0.5% BSA (molecular grade BSA from Biolabs or Acetylated BSA
692 from Ambion), and Tween-20 at 0.1%. Donkey fluorescent-conjugated secondary antibodies
693 were used as described in the immunofluorescence experiments.
694
695 **Yeast two-hybrid experiments**

696 Two-hybrid plasmids containing the *Drosophila Egl* (Egl; CG4051) full-length (pEgl-AD and
697 pEgl-BD), *BicD* full-length (pBicD-AD and pBicD-BD) and the *BicD* carboxy-terminal
698 domain (CTD; amino acids 535–782) (pBicD(535–782)-BD and pBicD (535–782)-AD) were
699 previously described (Rashpa et al., 2017). *D-TACC* (CG9765) full-length; and *Chc*
700 (CG9012) full-length, a fragment containing amino acids 329-803, and another one bearing
701 amino acids 329–542 were cloned into the pOAD and or pOBD2 vectors (Cagney et al.,
702 2000) in-frame either with the activator domain (AD) or the DNA-binding domain (BD)

703 sequence of GAL4, respectively, to create the "prey" plasmids, pD-TACC-AD, pChc-AD,
704 pChc (329–803)-AD, and pChc(329–542)-AD, as well as the "bait" plasmids pChc-BD, pChc
705 (329–803)-BD and pChc (329–542)-BD. To produce the constructs D-TACC-Ala and D-
706 TACC-Asp, D-TACC Ser863 was mutated to an alanine and aspartic acid codon,
707 respectively, by site-directed mutagenesis. Changes were verified by sequencing. Interactions
708 between "bait" and "prey" proteins were detected following a yeast interaction-mating
709 method using the strains PJ69-4a and PJ69-4alpha (Cagney et al., 2000).
710 For all cases, diploid cells containing both AD and BD constructs were selected in media
711 lacking tryptophan and leucine (–(L,W), *Growth test*). To test for possible interactions, cells
712 were further replica-plated in media lacking leucine, tryptophan and adenine (–(L, W, a),
713 media lacking leucine, tryptophan, histidine, and adenine (-(L,W,H,a), or media lacking
714 leucine, tryptophan, and histidine, and containing the indicated amounts of 3-Amino-1,2,4-
715 triazole (3AT), (-(*Interaction test*). For each test, ten-fold serial dilutions are presented.
716 Growth was scored after 4-5 days of growth at 30°C.
717

718 ***C. elegans* strains, RNAi and imaging**

719 N2, JDU233 (*H2B::mCherry;α-tubulin::GFP*), VJ512, *chc-1(tm2866)III/hT2[bli-4(e937) let-*
720 *?(q782) qIs48](I;III)*. Feeding of worms with dsRNA was performed on NGM plates
721 containing 1mM IPTG and carbenicillin using clones from the Ahringer RNAi library
722 (Kamath and Ahringer, 2003). For non-lethal phenotypes, the progeny was imaged after 60
723 hours of feeding of gravid adults at 20°C. For lethal phenotypes, L3/L4 larvae were
724 transferred onto RNAi plates and incubated for 12 h at room temperature to obtain gravid
725 adults. The empty vector L4440 was used as a control. Embryo dissections were performed as
726 previously described (Bellanger et al., 2007), and embryos were imaged immediately on an
727 agar pad using an AxioVision (Zeiss) microscope with a 100x NA 1.4 oil objective with a
728 GFP and an mCherry filter set. One plane was acquired every 10 seconds using Visiview, and
729 images were processed using ImageJ and Photoshop.

ACKNOWLEDGEMENTS

We thank S. Bullock, C. Bazinet, J. Hirst**,** J. Raff, T. Melgraw, H. Ohkura, G. Rogers, C. Sunkel, M. Affolter, E. Caussinus, the Bloomington *Drosophila* Stock Center (NIH P400D018537), and the Developmental Studies Hybridoma Bank (created by the NICHD of the NIH and maintained at The University of Iowa, Department of Biology, Iowa City, IA 52242) for constructs, fly stocks and antibodies. We thank FlyBase (U41HG000739) for the *Drosophila* genomic resources. We thank Andrew Swan for his scientific advice on how to study female meiosis and Yury Belyaev for his help with image processing.

This work was supported by funding's from the Swiss National Science Foundation (SNF, project grant 31003A_173188; www.snf.ch) and the University of Bern (www.unibe.ch) to BS, an SNF grant (project grant IZCOZ0_189884/31003A_176226) to P.M. and an Equal Opportunity grant from the Phil.-Nat. faculty to P.V.P. (www.unibe.ch).

Competing interests. The authors declare no competing financial interests.

Author contributions. P.V.P., D. B., G.S., G. H., G. M., and D. H performed experiments. P.V.P., G. S., P.M., and G.H. analyzed data. P.V. P. and B.S. conceived the studies. G.S. and P. M. contributed to writing the results of the *C. elegans* experiments. P.V.P and B.S. wrote the manuscript.

749 **REFERENCES**

750 **Basto, R., Scaerou, F., Mische, S., Wojcik, E., Lefebvre, C., Gomes, R., Hays, T. and**
751 **Karess, R.** (2004). In vivo dynamics of the rough deal checkpoint protein during
752 *Drosophila* mitosis. *Curr. Biol.* **14**, 56–61.

753 **Bazinet, C., Katzen, A. L., Morgan, M., Mahowald, A. P. and Lemmon, S. K.** (1993). The
754 *Drosophila* clathrin heavy chain gene: clathrin function is essential in a multicellular
755 organism. *Genetics* **134**, 1119–1134.

756 **Bellanger, J.-M., Carter, J. C., Phillips, J. B., Canard, C., Bowerman, B. and Gönczy, P.**
757 (2007). ZYG-9, TAC-1 and ZYG-8 together ensure correct microtubule function
758 throughout the cell cycle of *C. elegans* embryos. *Journal of Cell Science* **120**, 2963–
759 2973.

760 **Berleth, T., Burri, M., Thoma, G., Bopp, D., Richstein, S., Frigerio, G., Noll, M. and**
761 **Nüsslein-Volhard, C.** (1988). The role of localization of *bicoid* RNA in organizing the
762 anterior pattern of the *Drosophila* embryo. *EMBO J.* **7**, 1749–1756.

763 **Biot E, Crowell E, Höfte H, Maurin Y, Vernhettes S & Andrey P**. (2008). A new filter for
764 spot extraction in *N*-dimensional biological imaging. In *Fifth IEEE International*
765 *Symposium on Biomedical Imaging (ISBI'08): From Nano to Macro*, pp. 975-978.

766 **Booth, D. G., Hood, F. E., Prior, I. A. and Royle, S. J.** (2011). A TACC3/ch-TOG/clathrin
767 complex stabilises kinetochore fibres by inter-microtubule bridging. *EMBO J.* **30**, 906–
768 919.

769 **Brodsky, F. M.** (2012). Diversity of clathrin function: new tricks for an old protein. *Annu.*
770 *Rev. Cell Dev. Biol.* **28**, 309–336.

771 **Bullock, S. L. and Ish-Horowicz, D.** (2001). Conserved signals and machinery for RNA
772 transport in *Drosophila* oogenesis and embryogenesis. *Nature* **414**, 611–616.

773 **Buster, D. W., Daniel, S. G., Nguyen, H. Q., Windler, S. L., Skwarek, L. C., Peterson,**
774 **M., Roberts, M., Meserve, J. H., Hartl, T., Klebba, J. E., et al.** (2013). SCFSlimb
775 ubiquitin ligase suppresses condensin II-mediated nuclear reorganization by degrading
776 Cap-H2. *J Cell Biol* **201**, 49–63.

777 **Cagney, G., Uetz, P. and Fields, S.** (2000). High-throughput screening for protein-protein
778 interactions using two-hybrid assay. *Meth. Enzymol.* **328**, 3–14.

779 **Caussinus, E., Kanca, O. and Affolter, M.** (2011). Fluorescent fusion protein knockout
780 mediated by anti-GFP nanobody. *Nature Publishing Group* **19**, 117–121.

781 **Cullen, C. F., Deák, P., Glover, D. M. and Ohkura, H.** (1999). *mini spindles*: A gene
782 encoding a conserved microtubule-associated protein required for the integrity of the
783 mitotic spindle in *Drosophila. J Cell Biol* **146**, 1005–1018.

784 **Défachelles, L., Hainline, S. G., Menant, A., Lee, L. A. and Karess, R. E.** (2015). A
785 maternal effect *rough deal* mutation suggests that multiple pathways regulate *Drosophila*
786 RZZ kinetochore recruitment. *Journal of Cell Science* **128**, 1204–1216.

787 **Dernburg A. F.** (2000) *In Situ* hybridization to somatic chromosomes. In: *Drosophila*
788 Protocols (ed. W. Sullivan, M. Ashburner and R. S. Hawley), pp. 24–55. Cold Spring
789 Harbor, New York, USA: Cold Spring Harbor Laboratory Press.

790 **Dienstbier, M., Boehl, F., Li, X. and Bullock, S. L.** (2009). Egalitarian is a selective RNA-
791 binding protein linking mRNA localization signals to the dynein motor. *Genes Dev.* **23**,
792 1546–1558.

793 **Driever, W. and Nüsslein-Volhard, C.** (1988). A gradient of bicoid protein in *Drosophila*
794 embryos. *Cell* **54**, 83–93.

795 **Ferree, P. M. and Barbash, D. A.** (2009). Species-specific heterochromatin prevents mitotic
796 chromosome segregation to cause hybrid lethality in *Drosophila. PLoS Biol.* **7**,
797 e1000234.

798 **Fischer, M. G., Heeger, S., Häcker, U. and Lehner, C. F.** (2004). The mitotic arrest in
799 response to hypoxia and of polar bodies during early embryogenesis requires *Drosophila*
800 *Mps1. Curr. Biol.* **14**, 2019–2024.

801 **Fu, W., Tao, W., Zheng, P., Fu, J., Bian, M., Jiang, Q., Clarke, P. R. and Zhang, C.**
802 (2010). Clathrin recruits phosphorylated TACC3 to spindle poles for bipolar spindle
803 assembly and chromosome alignment. *Journal of Cell Science* **123**, 3645–3651.

804 **Fumoto, K., Hoogenraad, C. C. and Kikuchi, A.** (2006). GSK-3beta-regulated interaction
805 of BICD with dynein is involved in microtubule anchorage at centrosome. *EMBO J.* **25**,
806 5670–5682.

807 **Gergely, F., Kidd, D., Jeffers, K., Wakefield, J. G. and Raff, J. W.** (2000). D-TACC: a
808 novel centrosomal protein required for normal spindle function in the early *Drosophila*
809 embryo. *EMBO J.* **19**, 241–252.

810 **Gönczy, P., Pichler, S., Kirkham, M. and Hyman, A. A.** (1999). Cytoplasmic dynein is
811 required for distinct aspects of MTOC positioning, including centrosome separation, in
812 the one cell stage *Caenorhabditis elegans* embryo. *J Cell Biol* **147**, 135–150.

813 **Heerssen, H., Fetter, R. D. and Davis, G. W.** (2008). Clathrin dependence of synaptic-
814 vesicle formation at the *Drosophila* neuromuscular junction. *Curr. Biol.* **18**, 401–409.

815 **Heuer, J. G., Li, K. and Kaufman, T. C.** (1995). The *Drosophila* homeotic target gene
816 *centrosomin (cnn)* encodes a novel centrosomal protein with leucine zippers and maps to
817 a genomic region required for midgut morphogenesis. *Development* **121**, 3861–3876.

818 **Hirst, J., Sahlender, D. A., Choma, M., Sinka, R., Harbour, M. E., Parkinson, M. and**
819 **Robinson, M. S.** (2009). Spatial and functional relationship of GGAs and AP-1 in
820 Drosophila and HeLa cells. *Traffic* **10**, 1696–1710.

821 **Hoogenraad, C. C. and Akhmanova, A.** (2016). Bicaudal D Family of Motor Adaptors:
822 Linking Dynein Motility to Cargo Binding. *Trends Cell Biol.* **26**, 327–340.

823 **Howell, B. J., McEwen, B. F., Canman, J. C., Hoffman, D. B., Farrar, E. M., Rieder, C.**
824 **L. and Salmon, E. D.** (2001). Cytoplasmic dynein/dynactin drives kinetochore protein
825 transport to the spindle poles and has a role in mitotic spindle checkpoint inactivation. *J*
826 *Cell Biol* **155**, 1159–1172.

827 **Kamath, R. S. and Ahringer, J.** (2003). Genome-wide RNAi screening in Caenorhabditis

828 elegans. *Methods* **30**, 313–321.

829 **Kao, L.-R. and Megraw, T. L.** (2009). Centrocortin Cooperates with Centrosomin to
830 Organize *Drosophila* Embryonic Cleavage Furrows. *Curr. Biol.* **19**, 937–942.

831 **Kasprowicz, J., Kuenen, S., Miskiewicz, K., Habets, R. L. P., Smitz, L. and Verstreken,**
832 **P.** (2008). Inactivation of clathrin heavy chain inhibits synaptic recycling but allows bulk
833 membrane uptake. *J Cell Biol* **182**, 1007–1016.

834 **Kellogg, D. R., Mitchison, T. J. and Alberts, B. M.** (1988). Behaviour of microtubules and
835 actin filaments in living *Drosophila* embryos. *Development* **103**, 675–686.

836 **Koch, R., Ledermann, R., Urwyler, O., Heller, M. and Suter, B.** (2009). Systematic
837 functional analysis of Bicaudal-D serine phosphorylation and intragenic suppression of a
838 female sterile allele of *BicD*. *PLoS ONE* **4**, e4552.

839 **Li, X., Kuromi, H., Briggs, L., Green, D. B., Rocha, J. A. O. J., Sweeney, S. T. and**
840 **Bullock, S. L.** (2010). Bicaudal-D binds clathrin heavy chain to promote its transport and
841 augments synaptic vesicle recycling. *EMBO J.* **29**, 992–1006.

842 **Lin, C.-H., Hu, C.-K. and Shih, H.-M.** (2010). Clathrin heavy chain mediates TACC3
843 targeting to mitotic spindles to ensure spindle stability. *J Cell Biol* **189**, 1097–1105.

844 **Logarinho, E., Bousbaa, H., Dias, J. M., Lopes, C., Amorim, I., Antunes-Martins, A. and**
845 **Sunkel, C. E.** (2004). Different spindle checkpoint proteins monitor microtubule
846 attachment and tension at kinetochores in *Drosophila* cells. *Journal of Cell Science* **117**,
847 1757–1771.

848 **Mach, J. M. and Lehmann, R.** (1997). An Egalitarian-BicaudalD complex is essential for
849 oocyte specification and axis determination in *Drosophila*. *Genes Dev.* **11**, 423–435.

850 **Margolis, J. S., Borowsky, M., Shim, C. W. and Posakony, J. W.** (1994). A small region
851 surrounding the distal promoter of the *hunchback* gene directs maternal expression. *Dev.*
852 *Biol.* **163**, 381–388.

853 **Nag, R. N., Niggli, S., Sousa-Guimarães, S., Vazquez-Pianzola, P. and Suter, B.** (2018).
854 *Mms19* is a mitotic gene that permits Cdk7 to be fully active as a Cdk-activating kinase.
855 *Development* **145**, dev156802.

856 **Paré, C. and Suter, B.** (2000). Subcellular localization of Bic-D::GFP is linked to an
857 asymmetric oocyte nucleus. *Journal of Cell Science* **113 (Pt 12)**, 2119–2127.

858 **Payne, C., Rawe, V., Ramalho-Santos, J., Simerly, C. and Schatten, G.** (2003).
859 Preferentially localized dynein and perinuclear dynactin associate with nuclear pore
860 complex proteins to mediate genomic union during mammalian fertilization. *Journal of*
861 *Cell Science* **116**, 4727–4738.

862 **Pérez-Mongiovi, D., Malmanche, N., Bousbaa, H. and Sunkel, C.** (2005). Maternal
863 expression of the checkpoint protein BubR1 is required for synchrony of syncytial
864 nuclear divisions and polar body arrest in *Drosophila melanogaster. Development* **132**,
865 4509–4520.

866 **Radford, S. J. and McKim, K. S.** (2016). Techniques for Imaging Prometaphase and
867 Metaphase of Meiosis I in Fixed *Drosophila* Oocytes. *J Vis Exp* e54666.

Ran, B., Bopp, R. and Suter, B. (1994). Null alleles reveal novel requirements for *Bic-D* during *Drosophila* oogenesis and zygotic development. *Development* **120**, 1233–1242.

Rashpa, R., Vazquez-Pianzola, P., Colombo, M., Hernandez, G., Beuchle, D., Berger, F., Peischl, S., Bruggmann, R. and Suter, B. (2017). *Cbp80* is needed for the expression of piRNA components and piRNAs. *PLoS ONE* **12**, e0181743.

Rieder, C. L. and Maiato, H. (2004). Stuck in division or passing through: what happens when cells cannot satisfy the spindle assembly checkpoint. *Dev. Cell* **7**, 637–651.

Royle, S. J. (2012). The role of clathrin in mitotic spindle organisation. *Journal of Cell Science* **125**, 19–28.

Royle, S. J. and Lagnado, L. (2006). Trimerisation is important for the function of clathrin at the mitotic spindle. *Journal of Cell Science* **119**, 4071–4078.

Royle, S. J., Bright, N. A. and Lagnado, L. (2005). Clathrin is required for the function of the mitotic spindle. *Nature* **434**, 1152–1157.

Sallés, F. J., Lieberfarb, M. E., Wreden, C., Gergen, J. P. and Strickland, S. (1994). Coordinate initiation of *Drosophila* development by regulated polyadenylation of maternal messenger RNAs. *Science* **266**, 1996–1999.

Sawicka, A. and Seiser, C. (2012). Histone H3 phosphorylation - a versatile chromatin modification for different occasions. *Biochimie* **94**, 2193–2201.

Schulz, C. and Tautz, D. (1995). Zygotic *caudal* regulation by *hunchback* and its role in abdominal segment formation of the *Drosophila* embryo. *Development* **121**, 1023–1028.

So, C., Seres, K. B., Steyer, A. M., Mönnich, E., Clift, D., Pejkovska, A., Möbius, W. and Schuh, M. (2019). A liquid-like spindle domain promotes acentrosomal spindle assembly in mammalian oocytes. *Science* **364**, eaat9557.

Sokac, A. M. and Wieschaus, E. (2008). Local actin-dependent endocytosis is zygotically controlled to initiate *Drosophila* cellularization. *Dev. Cell* **14**, 775–786.

Suter, B. and Steward, R. (1991). Requirement for phosphorylation and localization of the Bicaudal-D protein in *Drosophila* oocyte differentiation. *Cell* **67**, 917–926.

Suter, B., Romberg, L. M. and Steward, R. (1989). *Bicaudal-D*, a *Drosophila* gene involved in developmental asymmetry: localized transcript accumulation in ovaries and sequence similarity to myosin heavy chain tail domains. *Genes Dev.* **3**, 1957–1968.

Swan, A. and Suter, B. (1996). Role of *Bicaudal-D* in patterning the *Drosophila* egg chamber in mid-oogenesis. *Development* **122**, 3577–3586.

Vazquez-Pianzola, P. and Suter, B. (2012). Conservation of the RNA Transport Machineries and Their Coupling to Translation Control across Eukaryotes. *Comp. Funct. Genomics* **2012**, 287852–13.

Vazquez-Pianzola, P., Adam, J., Haldemann, D., Hain, D., Urlaub, H. and Suter, B. (2014). Clathrin heavy chain plays multiple roles in polarizing the *Drosophila* oocyte downstream of *Bic-D*. *Development* **141**, 1915–1926.

Vazquez-Pianzola P., Suter B., Hernández G. (2016) Evolution of the Molecules Coupling

907 mRNA Transport with Translational Control in Metazoans. In: Evolution of the Protein
908 Synthesis Machinery and Its Regulation (ed. G.Hernández R. Jagus), pp. 531-546. New
909 York.

910 **Vazquez-Pianzola, P., Schaller, B., Colombo, M., Beuchle, D., Neuenschwander, S.,**
911 **Marcil, A., Bruggmann, R. and Suter, B.** (2017). The mRNA transportome of the
912 BicD/Egl transport machinery. *RNA Biol* **14**, 73–89.

913 **Vazquez-Pianzola, P., Urlaub, H. and Suter, B.** (2011). Pabp binds to the *osk* 3'UTR and
914 specifically contributes to *osk* mRNA stability and oocyte accumulation. *Dev. Biol.* **357**,
915 404–418.

916 **Wharton, R. P. and Struhl, G.** (1989). Structure of the *Drosophila* BicaudalD protein and
917 its role in localizing the posterior determinant *nanos. Cell* **59**, 881–892.

918 **Wojcik, E., Basto, R., Serr, M., Scaërou, F., Karess, R. and Hays, T.** (2001). Kinetochore
919 dynein: its dynamics and role in the transport of the Rough deal checkpoint protein. *Nat.*
920 *Cell Biol.* **3**, 1001–1007.

921

922 **FIGURE LEGENDS**

923 **Figure 1. Dynamic localization of BicD and Chc with enrichment at embryonic spindles**
924 **and centrosomes. (A)** BicD (red), colocalized with the pericentrosomal marker Cnn (green)
925 and it is also present at metaphase spindles. Wild-type embryos in nuclear cycle 10 (NC10)
926 (a), NC12 (b) and during cellularization (NC14) (c) are shown. **(B)** *BicD*^{null}*, BicD::GFP*
927 stained with anti-GFP (green) and anti-α-tubulin (red) antibodies. An NC10 embryo is shown.
928 **(C)** Chc::V5 expressing embryos stained for V5 (red) and Cnn (green). A cellular blastoderm
929 (a) and an embryo in metaphase of NC13 are shown (b). **(D)** Live imaging of Chc::mCherry
930 expressing embryos. **(E)** Chc::mCherry, detected with anti-mCherry antibodies (red), is
931 present along both MII tandem spindles (arrows) and at the central aster (arrowhead). **(F)**
932 During MII, BicD::GFP (detected with anti-GFP antibodies) is enriched in the region of the
933 tandem spindles (arrow marks the most superficial spindle) and the central aster (arrowhead)
934 above cytoplasmic levels. Embryos in E-F were also stained for anti-α-tubulin (red in E,
935 green in F). In A-C, E-F, DNA was also stained with Hoechst (blue).
936

937 **Figure 2. *hb-deGradFP* degrades BicD::GFP specifically in freshly laid eggs, causing**
938 **early developmental arrest. (A)** Scheme depicting the construct expressed in flies. **(B)** RNA
939 FISH detects the *deGradFP* mRNA (red) enriched in the anterior region of freshly laid
940 embryos. **(C)** The deGradFP construct (red signal) is ubiquitously present in young embryos.
941 Wild-type embryos without the *deGradFP* transgene were used as negative controls in B and
942 C. **(D)** Percentage of embryos of the depicted maternal genotype that hatched as larvae. **(E)**
943 Percentage of normally developed embryos laid by the indicated mothers. **(F-I)** Ovaries and
944 embryos produced from control (*BicD::GFP, BicD*^{null}) and *BicD*$^{hb\text{-}deGradFP}$ females were used.
945 **(F)** Shows BicD::GFP fluorescence signal (green). **(G)** BicD::GFP was detected using anti-
946 GFP antibodies (green). Embryos were staged by anti-α-tubulin staining (red). **(H-I)** Western
947 blots showing BicD::GFP and deGradFP levels in ovaries **(H)** and 0-2h old embryos **(I)**.
948 Increasing amounts of cytoplasmic extracts were loaded for each sample (loading control: α-

949 tubulin). Relative abundance of BicD::GFP/α-tubulin, normalized to the control, was
950 calculated for the last 2 lanes. Hoechst (blue) shows the DNA in IF experiments.
951
952 **Figure 3. Fertilized *BicD*$^{hb\text{-}deGradFP}$ embryos arrest at the start of embryogenesis with**
953 **abnormal spindles, over-replicated female meiotic products, and without pronuclear**
954 **fusion. (A-C)** 30-60 min old embryos with the indicated maternal genotypes stained for α-
955 tubulin (red), the centrosome marker Cnn (green), and DNA (blue). **A)** Percentage of embryos
956 displaying the different phenotypes. The genotypes of their mothers are indicated. Embryos
957 were characterized as unfertilized when no internal nuclei were seen and the 4 polar bodies,
958 arrange in rosette-like structures (mostly fused into a single one), were observed at the surface
959 of the embryo. Two independent collections (n1 and n2) were analyzed**.** Error bars show the
960 SD. For *BicD::GFP,* *BicD*^{null}*/BicD::GFP,* *BicD*^{null} *n1=84, n2=82.* For *BicD::GFP,*
961 *BicD*^{null}*/+; hb-deGradFP/hb-deGradFP n1=55, n2=70.* And for *BicD*$^{hb\text{-}deGradFP}$ *n1=42,*
962 *n2=63.* (**B-C***)* Examples of the observed phenotypes**. (B)** Normal nuclear divisions in a
963 control embryo (from a *BicD::GFP, BicD*^{null} mother)**. (C)** Overview of the spindles seen in
964 *BicD*$^{hb\text{-}deGradFP}$ embryos classified as "arrested with centrosomes" (a) or as "arrested,
965 acentrosomal" (b). **(D-G)** DNA FISH with X (white) and Y (red) chromosomal probes and
966 stained for α-tubulin (green) and DNA (blue). Arrows mark the sperm tails and arrowheads
967 free centrosomes. **(D)** Example of a control wild-type male embryo in the 2nd mitotic
968 metaphase. **(E-G)** Examples of arrested *BicD*$^{hb\text{-}deGradFP}$ male embryos. Images are z-stack
969 projections through the nuclei and yellow boxes mark the corresponding magnified nuclei.
970
971 **Figure 4. Female meiotic products fail to arrest in metaphase and undergo extra rounds**
972 **of replication in unfertilized *BicD*$^{hb\text{-}deGradFP}$ eggs.**
973 **(A)** 0-1 h old unfertilized eggs from the depicted mothers stained for α-tubulin (red) and
974 DNA (blue) and classified as follows. 1) eggs that apparently completed meiosis normally (up
975 to four rosette like structures that normally fuse into one single rosette); 2) eggs displaying a

976 normal metaphase II tandem spindle; 3) eggs presenting 1-2 rosette like structures plus 1-2
977 spindles (probably representing normal meiosis intermediate products); 4) eggs with a big
978 DNA blob surrounded by a star of microtubules (MT); 5) eggs containing one single nucleus/
979 big spindle; 6) eggs containing several spindles; 7) eggs with other defects. Most control eggs
980 (from wild type, *BicD::GFP, BicD*^{null} or *BicD::GFP, BicD*^{null}*/+; hb-deGradFP* mothers)
981 completed meiosis normally. In contrast, many eggs from *BicD*$^{hb\text{-}deGradFP}$ mothers contained
982 multiple spindles and, to a lesser extent, one big spindle. Error bars show the SD of three to
983 four independent egg collections (n1 to n4). For *wild type,* n1= 145, n2=95, n3=67;
984 for *BicD::GFP, BicD*^{null}*/BicD::GFP,* n1=92, n2=72, n3=147*;* for *BicD*^{null}, *BicD::GFP/ +; hb-*
985 *deGradFP /hb-deGradFP,* n1=68, n2=46, n3= 69, n4=67*;* for *BicD*$^{hb\text{-}deGradFP}$, *n1=29, n2=45,*
986 *n3=32* were scored. **(B-C)** Eggs from the same parents as in A) subjected to FISH to detect
987 the X chromosome (white) and stained for α-tubulin (red) and DNA (blue). **(B)** Examples of
988 control eggs (*BicD::GFP, BicD*^{null}), where the meiotic products have fused into a single (b) or
989 two rosette-like structures (b'), showing a total of four X chromosomes
990 signals. **(C)** (c) *BicD*$^{hb\text{-}deGradFP}$ egg with a single nucleus containing an abnormal rosette-like
991 structure, partially decondensed chromosomes, and many dotted X chromosomal signals.
992 (c') *BicD*$^{hb\text{-}deGradFP}$ egg with more than four meiotic products. Every nucleus contains many
993 dotted X chromosomal signals (C1-2). **(D-E)** Unfertilized wild-type and and *BicD*$^{hb\text{-}deGradFP}$
994 eggs stained for CID (green, marking centromeres), PH3 (red) and DNA (blue). 100% (12/12
995 confocal images) of the single fused rosette nuclei in control eggs showed strong PH3
996 staining along the entire chromosomes. Although these structures in *BicD*$^{hb\text{-}deGradFP}$ eggs were
997 also positive for PH3, in 90,9 % (10/11) of them the signal was only enriched at the
998 pericentromeric region. 86% (6/7 confocal images) of the single fused rosette-like nuclei in
999 control eggs showed normal CID staining. In contrast, 63.7 % (7/11) of these structures
1000 in *BicD*$^{hb\text{-}deGradFP}$ eggs showed an increased number of CID-positive dots. **(E)** Eggs were
1001 stained for α-tubulin (red), PH3 (green), and DNA (blue). Images are z-stack projections
1002 through the nuclei and yellow boxes mark the corresponding magnified nuclei.

1003 **Figure 5. BicD contributes to the recruitment of the SAC components BubR1 and Mad2**
1004 **to the female meiotic products.** 0-1 h old unfertilized eggs stained for α-tubulin (red), DNA
1005 (blue) and BubR1 **(A)** or Mad2 **(B)** (green). (**A) a)** Wild-type meiotic products fused into a
1006 single rosette showed BubR1 staining at the kinetochores. **b)** *BicD*$^{hb\text{-}deGradFP}$ egg containing a
1007 unique rosette-like polar body without BubR1 signals. **c)** *BicD*$^{hb\text{-}deGradFP}$ egg with only one
1008 polar body showing weak BubR1 signals. **d)** *BicD*$^{hb\text{-}deGradFP}$ egg with several meiotic products
1009 that are negative for BubR1. **d')** magnified images of the indicated nuclei in d). **(B) a)** Single
1010 polar body rosette structure in a control egg (*BicD::GFP, BicD*^{null}) with Mad2 at the
1011 kinetochores of the polar body. **b)** *BicD*$^{hb\text{-}deGradFP}$ egg where the unique rosette-like polar body
1012 lacks Mad2 signal. **c)** *BicD*$^{hb\text{-}deGradFP}$ egg with only one polar body that stains only weakly for
1013 Mad2. **d)** In this *BicD*$^{hb\text{-}deGradFP}$ egg, the female meiotic products have replicated and don't
1014 stain for Mad2. Images are z-stack projections through the nuclei.
1015
1016 **Figure 6. Proper localization of D-TACC, Msps, and clathrin at the MII tandem**
1017 **spindles requires BicD.** 5 min egg collections of controls (laid by homozygous *BicD::GFP,*
1018 *BicD*^{null} (B-C) or wild-type mothers for (A) and *BicD*$^{hb\text{-}deGradFP}$ embryos stained for α-tubulin
1019 (red) and either Clc **(A),** D-TACC **(B)** or Msps **(C)** (green). DNA is shown in blue. **(A)**
1020 Maximum intensity projection images subjected to depth correction (see Methods) are shown.
1021 Clc hyper-accumulates at the central aster (arrowhead) compared to the signal at the spindles
1022 (arrows) *in BicD*$^{hb\text{-}deGradFP}$eggs. (A') Percentage of embryos showing similar signal intensity
1023 along the tandem spindles (TS) and the central aster (CA) (CA ≈TS), and embryos with
1024 hyper-accumulation of Clc at the central aster (CA>>TS) is shown for both genotypes. n=
1025 sum of embryos scored for each genotype in two independent experiments. Two independent
1026 researchers performed the qualitative scoring blindly. **(B-C)** Maximum intensity projection
1027 images are shown. The spindle shown on top is the more superficial one in the embryo and its
1028 signal is stronger because the signal from the spindle below is often masked by the
1029 cytoplasmic signal above. D-TACC and Msps localized to the tandem spindles and to the

1030 central aster (arrowheads). Msps is also enriched at the minus end poles of the tandem
1031 spindles in control embryos (arrow in C). Compared to the signal intensity in the central aster,
1032 D-TACC and Msps signals on the *BicD*$^{hb\text{-}deGradFP}$ spindles are reduced. **(B', C')** The mean
1033 fluorescent signal intensity ratio (signal in the most superficial spindle vs signal in central
1034 aster) for D-TACC (B') and Msps (C') was quantified for each imaged MII and AII spindle.
1035 Data are presented as mean ± SD. Statistical significance and p values were determined by the
1036 Student's unpaired test. (B') Control: n=51, *BicD*$^{hb\text{-}deGradFP}$: n=36; 3 experiments. (C')
1037 Control: n=30, *BicD*$^{hb\text{-}deGradFP}$: n=34; 2 experiments.
1038
1039 **Figure 7. *Drosophila* Chc binds to D-TACC through the same domain it interacts with**
1040 **BicD, and *BicD* and *Chc* genetically interact in embryos.**
1041 **(A)** Yeast two-hybrid interaction tests. Full-length (FL) and partial Chc fragments (Chc$^{329\text{-}542}$
1042 and Chc$^{329\text{-}803}$), respectively, were fused to the DNA binding domain (BD). Full-length D-
1043 TACC wild type (WT) and *D-TACC*^{S863A} were fused to the activator domain (AD). Empty
1044 vectors served as negative controls. **(B)** IP of total embryo extracts expressing a Myc-tagged
1045 Chc fusion protein (Myc::Chc). Antibodies used for the IPs are indicated on top. Beads alone
1046 and anti-Myc pull-downs in wild-type (wt) embryo extracts were done as negative controls.
1047 Western blots of the precipitated material were tested for the presence of BicD, Clc, D-TACC
1048 and Myc::Chc. 0.15% of the cytoplasmic extract used for each IP was loaded as input. Bottom
1049 panel shows a longer exposure of the Myc::Chc blot. **(C-D)** Maternal genotypes are indicated.
1050 Percentage of embryos that hatched into larvae **(C)** and of developing embryos **(D)**.

Fig. 1

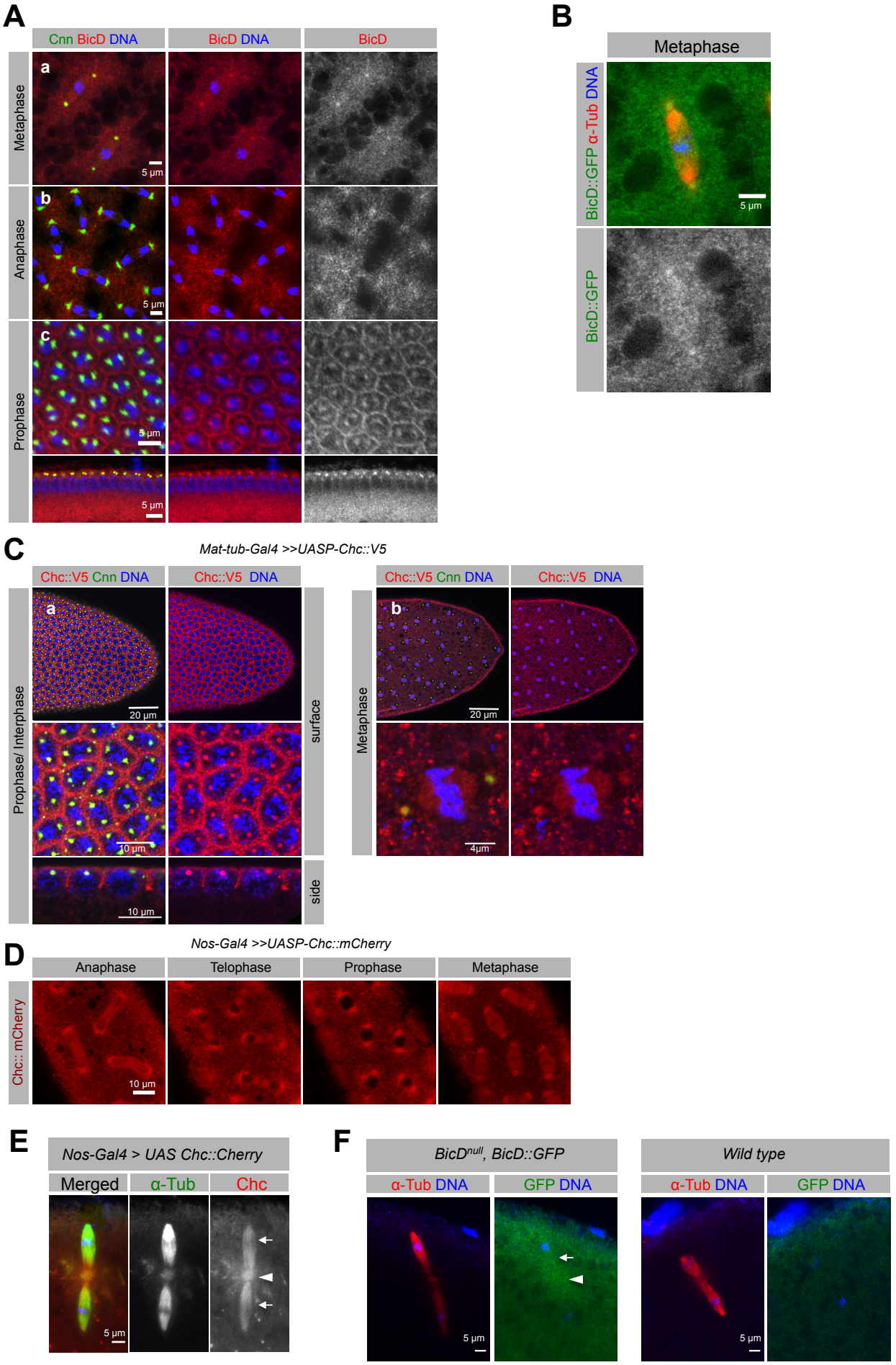
A
Cnn BicD DNA
BicD DNA
BicD
Metaphase
Anaphase
Prophase
a
b
c
5 µm
B
Metaphase
BicD::GFP α-Tub DNA
BicD::GFP
C
Mat-tub-Gal4 >>UASP-Chc::V5
Chc::V5 Cnn DNA
Chc::V5 DNA
Prophase/ Interphase
Metaphase
surface
side
20 µm
10 µm
4µm
D
Nos-Gal4 >>UASP-Chc::mCherry
Anaphase
Telophase
Prophase
Metaphase
Chc:: mCherry
E
Nos-Gal4 > UAS Chc::Cherry
Merged
α-Tub
Chc
F
BicD^null, BicD::GFP
Wild type
α-Tub DNA
GFP DNA

Fig. 2

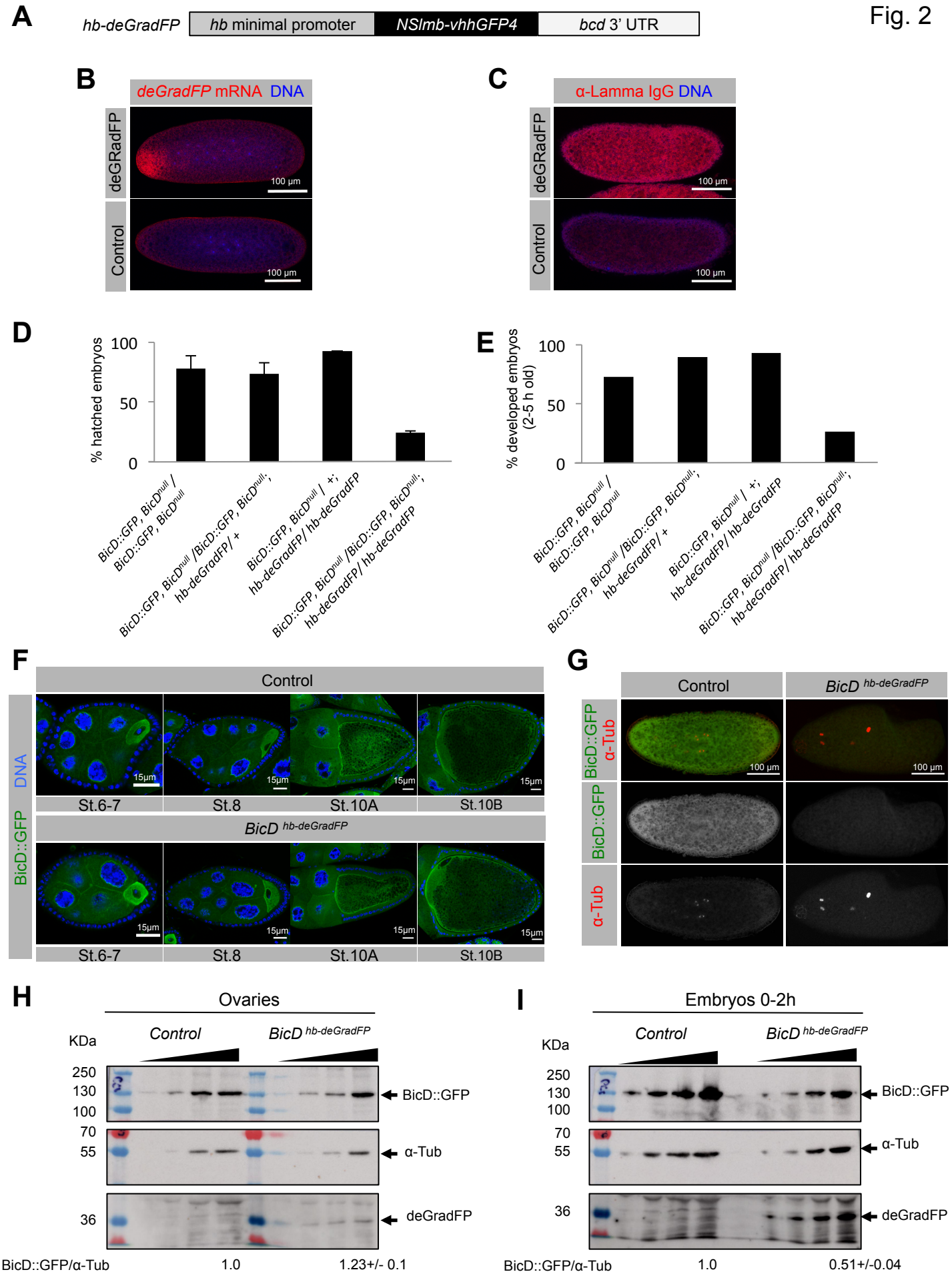
A
hb-deGradFP
hb minimal promoter
NSImb-vhhGFP4
bcd 3' UTR
B
deGradFP mRNA DNA
deGRadFP
Control
100 µm
C
α-Lamma IgG DNA
deGRadFP
Control
100 µm
D
% hatched embryos
100
50
0
BicD::GFP, BicDnull / BicD::GFP, BicDnull
BicD::GFP, BicDnull /BicD::GFP, BicDnull; hb-deGradFP/ +
BicD::GFP, BicDnull / +; hb-deGradFP/ hb-deGradFP
BicD::GFP, BicDnull /BicD::GFP, BicDnull; hb-deGradFP/ hb-deGradFP
E
% developed embryos (2-5 h old)
100
50
0
BicD::GFP, BicDnull / BicD::GFP, BicDnull
BicD::GFP, BicDnull /BicD::GFP, BicDnull; hb-deGradFP/ +
BicD::GFP, BicDnull / +; hb-deGradFP/ hb-deGradFP
BicD::GFP, BicDnull /BicD::GFP, BicDnull; hb-deGradFP/ hb-deGradFP
F
Control
DNA
BicD::GFP
15µm
St.6-7
St.8
St.10A
St.10B
BicD hb-deGradFP
G
Control
BicD hb-deGradFP
BicD::GFP α-Tub
BicD::GFP
α-Tub
100 µm
H
Ovaries
KDa
Control
BicD hb-deGradFP
250
130
100
70
55
36
BicD::GFP
α-Tub
deGradFP
BicD::GFP/α-Tub
1.0
1.23+/- 0.1
I
Embryos 0-2h
KDa
Control
BicD hb-deGradFP
250
130
100
70
55
36
BicD::GFP
α-Tub
deGradFP
BicD::GFP/α-Tub
1.0
0.51+/-0.04

Fig. 3

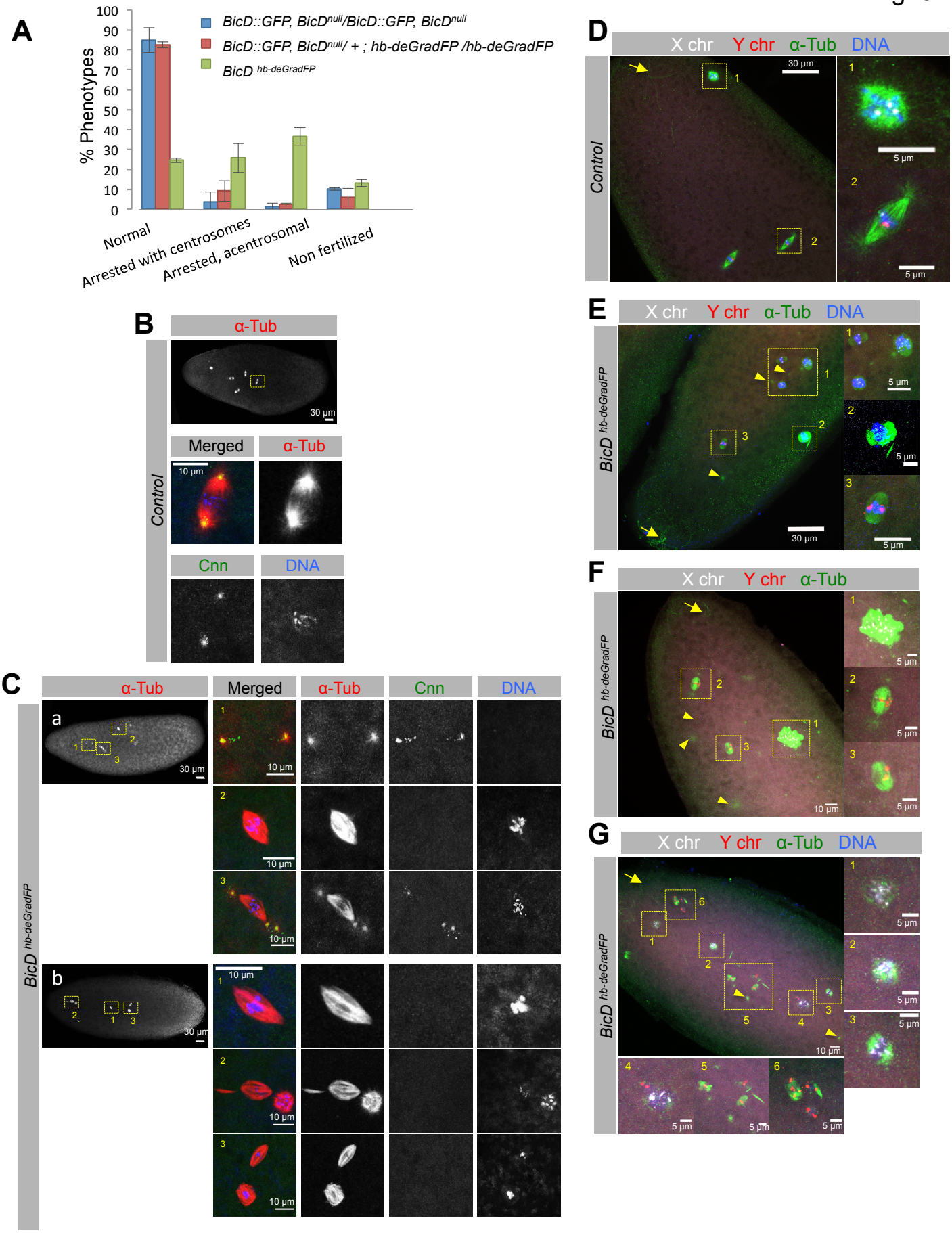
A
% Phenotypes
100
90
80
70
60
50
40
30
20
10
0
BicD::GFP, BicD^null/BicD::GFP, BicD^null
BicD::GFP, BicD^null/ + ; hb-deGradFP /hb-deGradFP
BicD hb-deGradFP
Normal
Arrested with centrosomes
Arrested, acentrosomal
Non fertilized
B
α-Tub
Control
30 µm
Merged
α-Tub
10 µm
Cnn
DNA
C
α-Tub
Merged
α-Tub
Cnn
DNA
BicD hb-deGradFP
a
b
30 µm
10 µm
D
X chr
Y chr
α-Tub
DNA
Control
30 µm
5 µm
E
X chr
Y chr
α-Tub
DNA
BicD hb-deGradFP
30 µm
5 µm
F
X chr
Y chr
α-Tub
BicD hb-deGradFP
10 µm
5 µm
G
X chr
Y chr
α-Tub
DNA
BicD hb-deGradFP
10 µm
5 µm

Fig. 4

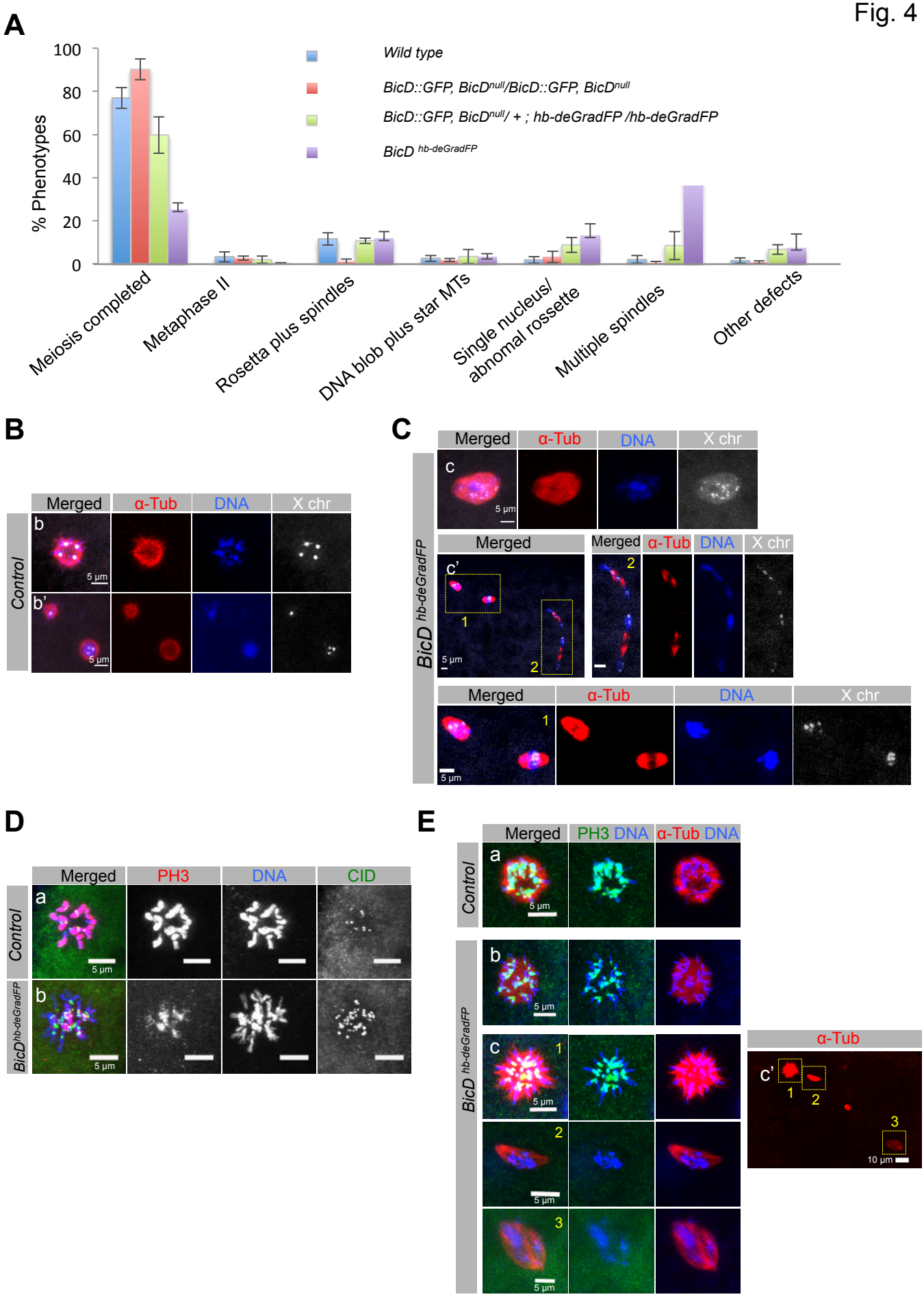
A
% Phenotypes
100
80
60
40
20
0
Wild type
BicD::GFP, BicD^null/BicD::GFP, BicD^null
BicD::GFP, BicD^null/ + ; hb-deGradFP /hb-deGradFP
BicD hb-deGradFP
Meiosis completed
Metaphase II
Rosetta plus spindles
DNA blob plus star MTs
Single nucleus/ abnomal rossette
Multiple spindles
Other defects
B
Merged
α-Tub
DNA
X chr
Control
b
b'
5 µm
C
BicD hb-deGradFP
c
c'
1
2
5 µm
D
Merged
PH3
DNA
CID
Control
BicD hb-deGradFP
a
b
5 µm
E
Merged
PH3 DNA
α-Tub DNA
Control
BicD hb-deGradFP
a
b
c
1
2
3
5 µm
α-Tub
c'
10 µm

Fig. 5

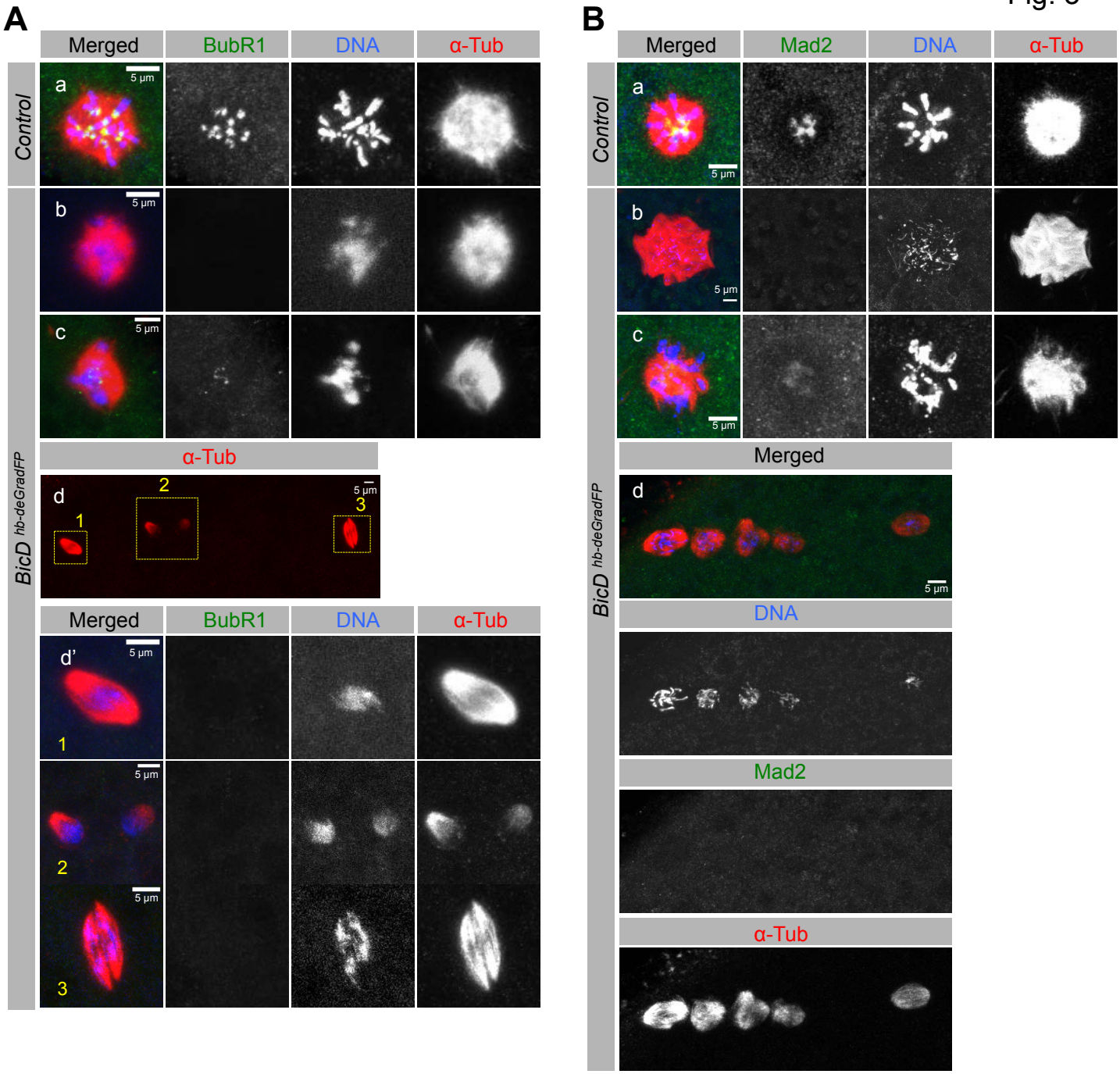
A
Merged
BubR1
DNA
α-Tub
Control
BicD hb-deGradFP
a
b
c
d
d'
1
2
3
5 µm
B
Merged
Mad2
DNA
α-Tub

Fig. 6

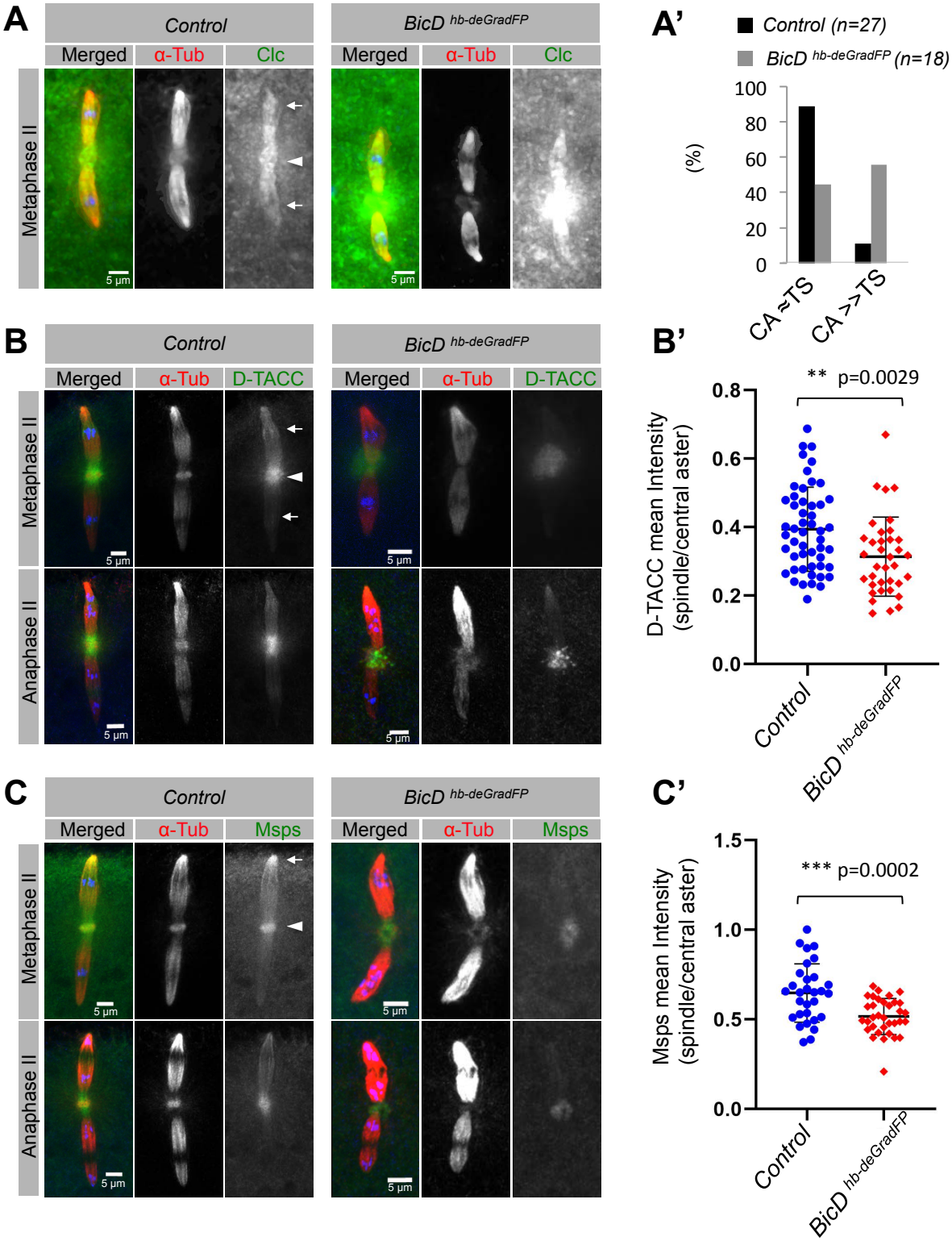
A
Control
BicD hb-deGradFP
Merged
α-Tub
Clc
Metaphase II
5 µm
A'
Control (n=27)
BicD hb-deGradFP (n=18)
(%)
100
80
60
40
20
0
CA≈TS
CA>>TS
B
D-TACC
Anaphase II
B'
** p=0.0029
D-TACC mean Intensity (spindle/central aster)
0.8
0.6
0.4
0.2
0.0
Control
BicD hb-deGradFP
C
Msps
C'
*** p=0.0002
Msps mean Intensity (spindle/central aster)
1.5
1.0
0.5
0.0

Fig. 7

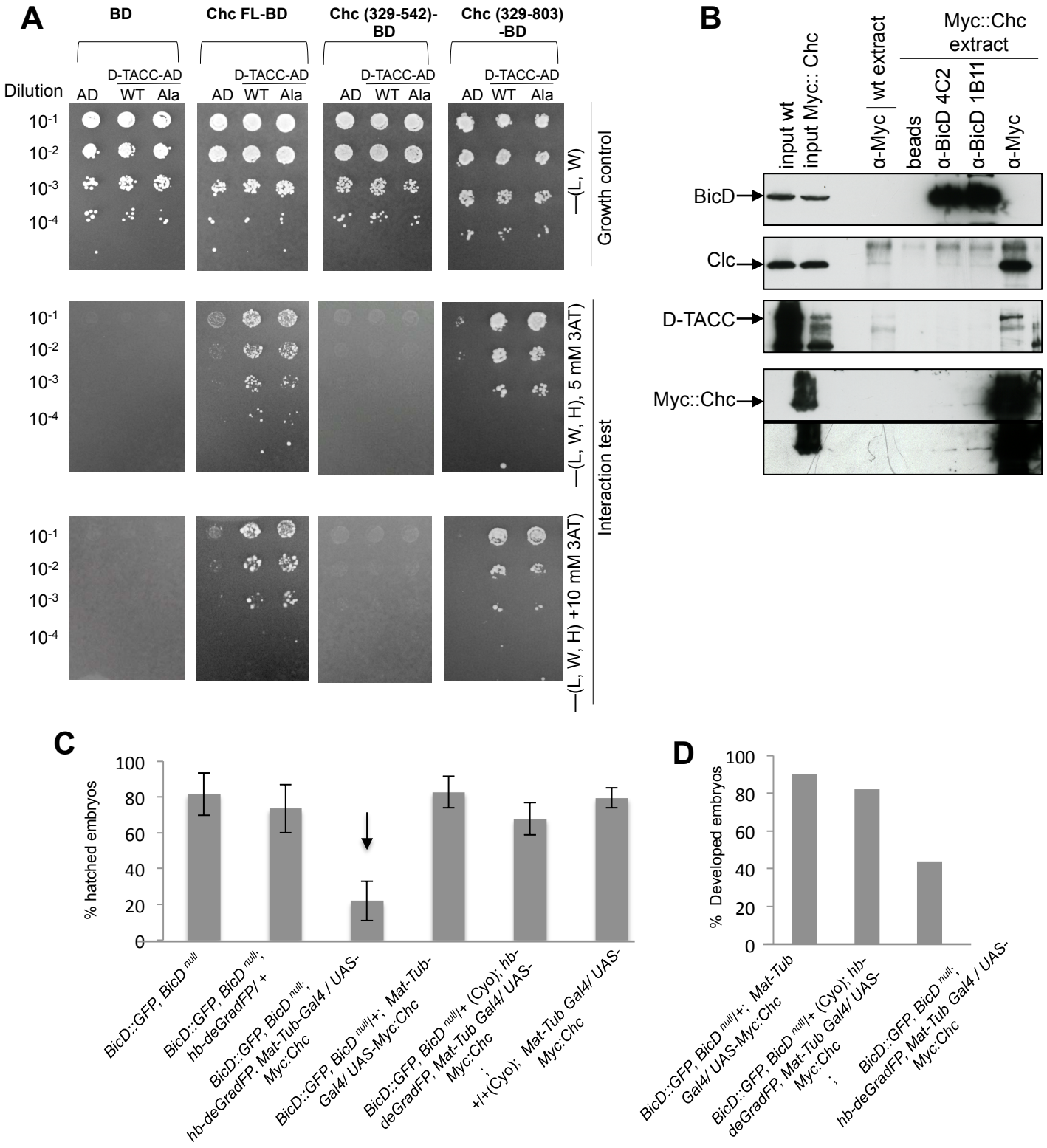
A
BD
Chc FL-BD
Chc (329-542)-BD
Chc (329-803)-BD
D-TACC-AD
AD
WT
Ala
Dilution
10-1
10-2
10-3
10-4
—(L, W)
Growth control
—(L, W, H), 5 mM 3AT)
—(L, W, H) +10 mM 3AT)
Interaction test
B
input wt
input Myc:: Chc
α-Myc
wt extract
Myc::Chc extract
beads
α-BicD 4C2
α-BicD 1B11
α-Myc
BicD
Clc
D-TACC
Myc::Chc
C
% hatched embryos
100
80
60
40
20
0
BicD::GFP, BicD null
BicD::GFP, BicD null, hb-deGradFP/ +
BicD::GFP, BicD null, hb-deGradFP, Mat-Tub-Gal4 / UAS-Myc:Chc
BicD::GFP, BicD null/+; Mat-Tub-Gal4/ UAS-Myc:Chc
BicD::GFP, BicD null/+ (Cyo); hb-deGradFP, Mat-Tub Gal4/ UAS-Myc:Chc
+/+(Cyo); Mat-Tub Gal4/ UAS-Myc:Chc
D
% Developed embryos
100
80
60
40
20
0
BicD::GFP, BicD null/+; Mat-Tub Gal4/ UAS-Myc:Chc
BicD::GFP, BicD null/+ (Cyo); hb-deGradFP, Mat-Tub Gal4/ UAS-Myc:Chc
BicD::GFP, BicD null, hb-deGradFP, Mat-Tub Gal4 / UAS-Myc:Chc